HHS Public Access

Author manuscript

Sci Signal. Author manuscript; available in PMC 2024 December 19.

Published in final edited form as:

Sci Signal. 2023 December 19; 16(816): eadh3449. doi:10.1126/scisignal.adh3449.

A non-canonical IRAK4-IRAK1 pathway counters DNA damage-induced apoptosis independently of TLR/IL-1R signaling

Yuanyuan Li[1,2,‡], **Richa B. Shah**[1,2,‡], **Samanta Sarti**[1,2], **Alicia L. Belcher**[1,2], **Brian J. Lee**[3], **Andrej Gorbatenko**[4,5,6], **Francesca Nemati**[1,2], **Honglin Yu**[1,2], **Zoe Stanley**[1,2], **Mahbuba Rahman**[1,2], **Zhengping Shao**[3], **Jose M. Silva**[4,5], **Shan Zha**[3,7], **Samuel Sidi**[1,2,4,*]

[1]Department of Medicine, Division of Hematology and Medical Oncology, Tisch Cancer Institute, Icahn School of Medicine at Mount Sinai, New York, NY 10029, USA

[2]Department of Cell, Developmental and Regenerative Biology, The Graduate School of Biomedical Sciences, Icahn School of Medicine at Mount Sinai, New York, NY 10029, USA

[3]Institute for Cancer Genetics, College of Physicians and Surgeons, Columbia University, New York, NY 10032, USA

[4]Department of Oncological Sciences, Icahn School of Medicine at Mount Sinai, New York, NY 10029, USA

[5]Department of Pathology, Icahn School of Medicine at Mount Sinai, New York, NY 10029, USA

[6]Current address: Department of Medical Biochemistry, Amsterdam UMC, University of Amsterdam, 1105 AZ, Amsterdam, The Netherlands

[7]Division of Pediatric Oncology, Hematology and Stem Cell Transplantation, Department of Pediatrics, College of Physicians and Surgeons, Columbia University, New York, NY 10032, USA

Abstract

Interleukin-1 receptor (IL-1R)-associated kinases (IRAKs) are core effectors of Toll-like receptors (TLRs) and IL-1R in innate immunity. Here, we found that IRAK4 and IRAK1 together inhibit DNA damage-induced cell death independently of TLR/IL-1R signaling. In human cancer cells exposed to double-strand breaks (DSBs) induced by ionizing radiation, IRAK4 was activated downstream of ATR kinase. Activated IRAK4 then formed a complex with and activated IRAK1. Formation of this complex required the E3 ubiquitin ligase Pellino1, acting structurally but not catalytically. Activation of IRAK1 occurred independently of extracellular signaling, intracellular TLRs and the TLR/IL-1R signaling adaptor MyD88. Once activated, IRAK1 translocated to the nucleus in a Pellino2-dependent manner. In the nucleus, IRAK1 bound to the PIDD1 subunit of the pro-apoptotic PIDDosome and interfered with platform assembly, thus supporting cell survival.

*Correspondence: samuel.sidi@mssm.edu.
‡These authors contributed equally.

Author contributions: Y.L. and R.B.S. performed most zebrafish and cell culture experiments, respectively, with contributions from S. Sarti. (IRAK4-pThr^{345}/Ser^{346} time course, Peli2 MO and importin studies), A.L.B. (IRAK1-pThr^{387} time course), A.G. and J.M.S. (CRISPR-Cas9 editing), F.N. (assistance with IRAK4-pThr^{345}/Ser^{346} IF), H.Y. (assistance with clonogenic assays), Z. Stanley (assistance with micro-IR image analysis), M.R. (assistance with IRAK1-pThr^{209} image analysis) and B.J.L, Z. Shao, and S.Z. (2-photon micro-IR treatments). S. Sidi conceived and supervised the study, and wrote the manuscript with Y.L., R.B.S and S. Sarti.

Competing Interests: The authors declare that they have no competing interests.

This non-canonical IRAK signaling pathway was also activated in response to bleomycin and topoisomerase inhibitors, as well as to sustained exposure to replication stress inducer aphidicolin that resulted in DSBs. In a zebrafish model of tumor radioresistance, the loss of IRAK4, its kinase activity, either Pellino, or the nuclear localization sequence in IRAK1 sensitized the fish to radiation. Thus, the findings may lead to strategies for overcoming tumor resistance to mainstay cancer treatments.

Introduction

Interleukin-1 receptor (IL-1R)-associated kinase 1 (IRAK1) is an evolutionarily conserved death domain (DD)-containing protein kinase whose *Drosophila* homolog, pelle, transduces dorso-ventral patterning and microbial cues recognized by the transmembrane receptor Toll (1–6). The immune function was found to be conserved in vertebrates, in which the kinase transduces pathogen cues recognized by Toll-like receptors (TLR) and IL-1R (7–10). As in flies, TLR/IL-1R-induced IRAK1 activation culminates in the activation of pro-inflammatory signaling cascades including NF-κB, p38 MAPK and JNK (9, 11), overall defining a core branch of innate immunity across species (12, 13).

The mechanism of IRAK1 activation by TLR/IL-1R was elucidated by several groups who identified Myeloid Differentiation Primary Response 88 (MyD88) (14), a protein of previously unknown function (15), as the adaptor molecule responsible for the recruitment of IRAK1 and its sister kinase, IRAK4, to the ligated receptors (16–19). MyD88 harbors a Toll/IL-1R homology (TIR) domain and a DD which respectively bind the receptor and IRAK kinases through homotypic TIR:TIR and DD:DD interactions, thus physically bridging the molecules. This results in the formation of the MyDDosome complex (MyD88-IRAK4-IRAK1) at the inner surface of the cell (20–23). The MyDDosome provides the necessary activation platform for IRAKs: Only once in the MyDDosome can IRAK4 dimerize and *trans*-autophosphorylate, resulting in its activation (23–26). This proximity-induced activation of IRAK4 is the key initiating step in IRAK1 activation, with most (20, 23–25, 27, 28) but not all (29) models implicating IRAK4-mediated phosphorylation of IRAK1 on residue T209 as responsible for IRAK1 activation. IRAK1 then fully activates via autophosphorylation on T387 in the activation loop and, in turn, dissociates from the MyDDosome (23, 27). To date, no pathway other than TLR/IL-1R has been reported to signal through IRAK1/4, and while TLRs can signal independently of MyD88, all TLR/IL-1R pathways that signal through IRAKs do so through MyD88 (9, 12).

The notion that IRAK kinases are confined to TLR and IL-1R signaling has been challenged by an unbiased screen in zebrafish that identified IRAK1 as essential for cell survival in response to ionizing radiation (IR) (30). This pro-survival signaling function is conserved in human cells, in which it appears to drive intrinsic tumor resistance to radiation therapy. Rather than signaling through NF-κB, p38 MAPK, JNK or ERK, IRAK1 was found to act—at least in part—by preventing IR-induced apoptosis mediated by the PIDDosome complex (PIDD-RAIDD-caspase-2) (31). Whereas IR-induced IRAK1 signaling appeared to involve IRAK4, it did not appear to require MyD88 (30). These observations suggested that IRAK1 might serve in a pathway distinct from the canonical, TLR/IL-1R axis. Here, we

present evidence in support of such a non-canonical pathway of IRAK1 signaling, which is responsible for sensing and transducing DNA damage into an anti-apoptotic response. Key distinguishing features include a distinct IRAK1 activation platform operating in the cytoplasm, not the cell surface, and distinct downstream signaling which requires rapid transport of the activated kinase from the cytoplasm into the nucleus.

Results

IR-induced IRAK1 signaling requires IRAK4 but not MyDDosome assembly

RNA interference (RNAi) studies in HeLa cells suggested that IRAK4, like IRAK1, is required for cell survival in response to IR and might function in the same, MyD88-independent pathway (30). We confirmed these results in additional cell lines (fig. S1A–B) and in an *IRAK4* knockout HeLa line obtained by CRISPR/Cas9 editing (Fig. 1, A -C). The radiosensitive phenotype of *IRAK4*$^{-/-}$ cells was rescued by wild-type (WT) but not kinase-deficient (D329A) FLAG-IRAK4 (Fig. 1C and fig. S1C) (32). These results were recapitulated in zebrafish *p53*$^{M214K/M214K}$ (*p53*$^{MK/MK}$) mutant embryos, a whole-animal model of tumor resistance to radiotherapy (33) in which IR-induced IRAK1 signaling was originally uncovered (30). Morpholino antisense oligonucleotide (MO)-mediated knockdown of Irak4, similar to that of Irak1 (30), strongly sensitized the mutant fish to IR, as evidenced by a marked uptake of the cell death marker acridine orange in developing spinal cords (Fig. 1D–G). These effects were on-target because a standard control MO (std MO) had no effect and because Irak4-depleted fish were rescued by co-injection with human *IRAK4* mRNA, but not by that encoding IRAK4^{D329A} (Fig. 1D and F). These experiments demonstrated an evolutionarily conserved pro-survival role for IRAK4 in irradiated cells and that this function requires IRAK4 catalytic activity, similar to previously observed for IRAK1 (30).

Should IRAK4 function in the same pathway as IRAK1, then IR would be expected to activate IRAK4 in a MyD88-independent manner (30). Most models of IRAK4 activation involve dimerization-induced, IRAK4 *trans*-autophosphorylation on multiple sites encompassing Thr^{345} and Ser^{346} (24–26). We tested an antibody to IRAK4-pThr^{345}/Ser^{346} in immunofluorescence assays. We first analyzed IL-1β-treated cells, which would be expected to activate IRAK4 at the cell surface via MyDDosome formation at ligated IL-1Rs. The IRAK4-pThr^{345}/Ser^{346} signals matched this prediction; signals were detected at the inner cell periphery from 5 min post-treatment on and were absent in *IRAK4*$^{-/-}$ cells (Fig. 1H) and MyD88-depleted cells (Fig. 1, I and J). These experiments identified the IRAK4-pThr^{345}/Ser^{346} antibody as a reliable marker of IRAK4 activation.

In response to IR, IRAK4 was activated with similar kinetics, with IRAK4-pThr^{345}/Ser^{346} signals first detected as early as 5 min after IR and peaking at 15 min (Fig. 1H). However, in contrast with IL-1β, IR led to IRAK4 activation not at the cell surface but in the cytoplasm (Fig. 1H), and the signal was unaffected by depletion of MyD88 (Fig. 1, I and J, and fig. S1D). The MyD88-independence of IR-induced IRAK4 activation was further confirmed by immunoblotting analysis (Fig. 1K). Together, the cytoplasmic localization of IR-induced IRAK4 autophosphorylation and its non-reliance on MyD88 provided independent support

for the existence of an alternate, MyDDosome-independent route to IRAK1/4 activation in human cells.

To verify this biochemically, we performed a series of co-immunoprecipitation assays. While IRAK1 associated with both MyD88 and IRAK4 in response to IL-1β, as expected, it associated with IRAK4 but not MyD88 after IR (Fig. 1L; endogenous pulldowns shown in Fig. 1M). Additionally, whereas MyD88 was required for the IRAK4-IRAK1 interaction in IL-1β-treated cells, again as expected, it was not after IR (Fig. 1N). Consistent with these data, an IRAK4 mutant that is unable to bind MyD88, IRAK4^{R12C} (32), rescued irradiated *IRAK4*$^{-/-}$ cells and Irak4-depleted zebrafish as effectively as IRAK4^{WT} (Fig. 1, C–F, and fig. S1C). Thus, although kinetically similar, the activation of IRAK4 by IR differs from that by IL-1β both spatially (cytoplasm vs. cell surface) and mechanistically (MyDDosome-independent vs. dependent).

Active IRAK1 accumulates in the nucleus of irradiated cells

Given the unexpected cytoplasmic localization of IR-induced IRAK4 activation, we sought to investigate that of its presumptive substrate, IRAK1, and product, IRAK1-pThr^{209}, in irradiated cells. To identify reliable markers, we again trialed several antibodies in IL-1β-treated cells, in which both the native and phosphorylated species should be detected at the inner cell surface within minutes of treatment. Antibodies to IRAK1 and IRAK1-pThr^{209} were identified which produced the expected IL-1β-induced cell surface signals in HeLa cells (Fig. 2, A and B; note the absence of signals in *IRAK1*$^{-/-}$ cells).

In response to IR, native IRAK1 was detected in the cytoplasm, not at the cell surface, and remained cytoplasmic throughout (Fig. 2B and fig. S2A). IRAK1-pThr^{209} was first detected in the cytoplasm at 5 min post-IR (Fig. 2A and fig. S2B), which was consistent with the localization of active IRAK4 and native IRAK1 in irradiated cells (Fig. 1G and fig. S2A). Strikingly however, by 15 min, IRAK1-pThr^{209} was detected exclusively in the nucleus (Fig. 2A, right), in sharp contrast with its cell-surface localization in IL-1β-treated cells (Fig. 2A, left). The IR-induced nuclear localization of IRAK1-pThr^{209} was confirmed in multiple cell lines (fig. S2, C and D) and was also observed in irradiated zebrafish (fig. S2E).

Irradiated HeLa cells analyzed between the 5- and 15- min timepoints showed varying levels of cytoplasmic and nuclear IRAK1-pThr^{209} foci. At 10 min, the activated kinase could be found both in the cytoplasm and nucleus (fig. S2B) or already exclusively in the nucleus (Fig. 2A). Double-staining with IRAK1 and IRAK1-pThr^{209} antibodies confirmed that the native kinase remained in the cytoplasm as the nuclear IRAK1-pThr^{209} signal progressively increased (Fig. 2, B and C). These observations provided evidence of a possible transport of activated IRAK1 into the nucleus (see Fig. 4 below). Nuclear accumulation of IRAK1-pThr^{209} peaked at 15 min, was retained for 6 hours, and declined by 12 to 24 hours (fig. S2, F and G).

Consistent with residue Thr^{209} being the target of IRAK4, IR-induced IRAK1-pThr^{209} signals were undetectable in IRAK4-depleted cells (Fig. 2D), *IRAK4*$^{-/-}$ cells (fig. S2I) and Irak4-depleted zebrafish embryos (Fig. 2, G–I). WT IRAK4 restored Thr^{209} phosphorylation in irradiated *IRAK4*$^{-/-}$ cells, whereas kinase-deficient IRAK4^{R329A} failed to do so,

confirming the requirement for IRAK4 catalytic activity (fig. S2, I and J). In contrast to IRAK4, MyD88 was not required for IRAK1 activation in either HeLa or zebrafish cells (Fig. 2, D–H and fig. S2H). IRAK4^{R12C}, which fails to bind MyD88 (32), restored IR-induced IRAK1 Thr^{209} phosphorylation in *IRAK4*$^{-/-}$ cells as efficiently as the WT kinase (fig. S2, I and J). Collectively, these results revealed the existence of an evolutionarily conserved, MyD88-independent route to IRAK1 activation by IRAK4. This distinct IRAK signaling axis can be activated by IR and operates with similar kinetics to the canonical, TLR–IL-1R pathway, but in a spatially distinct manner.

IR-induced IRAK1 activation triggers its autophosphorylation in the nucleus

Biochemical and structural evidence suggests that once phosphorylated by IRAK4 on Thr^{209}, IRAK1 autophosphorylates on Thr^{387} within the activation loop to achieve full activation (23, 27). A commercially available antibody raised against IRAK1-pThr^{387} produced nuclear signals in irradiated HeLa cells reminiscent of the IRAK1-pThr^{209} stains shown above (Fig. 3, A–B, I and J; five additional cell lines shown in fig. S3A). IR-induced nuclear IRAK1-pThr^{387} foci were absent in *IRAK1*$^{-/-}$ cells and were restored via transfection of IRAK1^{WT} but not an IRAK1 variant lacking the target threonine, IRAK1^{T387A} (27), validating antibody specificity (Fig. 3, C–E and I, and fig. S3B). Importantly, kinase-dead (KD) and phosphomutant T209A IRAK1 variants (27) also failed to restore the anti-pThr^{387} signals whereas phosphomimetic IRAK1^{T209D} enhanced immunoreactivity compared to WT (Fig. 3, F–I). These data indicated that IRAK1-pThr^{387} signals require both the activation and catalytic activity of IRAK1 and, thus, reflect autophosphorylation.

Examination of irradiated HeLa cells over time revealed discrete changes in the spatial distribution of IRAK1-pThr^{387} signals within the nucleoplasm (Fig. 3J). The signal was first detected at the inner nuclear periphery (within 1 μm of the nuclear envelope), then spread throughout the nucleoplasm and eventually concentrated in discrete nuclear areas (Fig. 3J). Co-staining for nucleolin and fibrillarin identified nucleoli as the destination of fully active IRAK1 (Fig. 3, K and L, and fig. S3, C and D). The localization of IRAK1-pThr^{387} to nucleoli reflected a specific process, because partially active IRAK1 (IRAK1-pThr^{209}) remained dispersed in the nucleoplasm (Fig. 3K, bottom, and fig. S3, C–E). The significance of the nucleolus to IR-induced IRAK1 signaling are addressed below.

Similar to IRAK1^{KD} and IRAK1^{T209A}, IRAK1^{T387A} failed to rescue *irak1* deficiency in irradiated *p53* mutant embryos (Fig. 3, M and N). Thus, IRAK1 autophosphorylation on Thr^{387} is necessary for IR-induced IRAK1 signaling. IRAK1^{T387A} did retain residual activity as compared to IRAK1^{KD} (Fig. 3N, bars 4 vs. 15 and 8, respectively). This partial rescue indicated that although autophosphorylation on Thr^{387} is necessary for IR-induced IRAK1 signaling, it is unlikely the sole catalytic target of IRAK1 in the pathway.

Nuclear translocation of active IRAK1 is essential for IR-induced IRAK1 signaling

Collectively, the data above supported a model for the early stages of IR-induced IRAK signaling where activation of IRAK4 in the cytoplasm leads to activation of IRAK1 therein, followed by its transport into—and full activation within—the nucleus. This was first

supported by RNAi experiments in HeLa cells which indicated that nuclear accumulation of IRAK1-pThr^{209} is sensitive to importin α/β dosage (fig. S4, A and B). Nuclear translocation of active IRAK1 would be a defining feature of IR-induced IRAK1 signaling which, alongside the lack of reliance on MyD88, would distinguish the pathway from TLR–IL-1R signaling. We thus tested whether nuclear transport even occurs, and if so, whether it is necessary for IR-induced IRAK1 signaling.

Examination of mammalian IRAK1 sequences revealed a candidate nuclear localization sequence (NLS), RRAKRR, located at the distal end of the kinase domain which, notably, is conserved in zebrafish (Fig. 4A). To disrupt the putative NLS, we mutated all arginines to alanine, thus generating an AAAKAA (R4A) IRAK1 variant. Introduction of FLAG-IRAK1^{R4A} into *IRAK1*$^{-/-}$ HeLa cells led to markedly reduced nuclear IRAK1-pThr^{209} and IRAK1-pThr^{387} signals after IR, with both the partially and fully activated species now trapped in the cytoplasm (Fig. 4, B–D, and fig. S4D). Notably, the R4A mutations did not compromise IRAK1 catalytic activity: IR-induced autophosphorylation on Thr^{387} was preserved in the variant, albeit occurring in the cytoplasm instead of the nucleus (Fig. 4, B–D and fig. S4, C and D). Thus, IRAK1^{R4A} represented a true separation-of-function mutant which uncoupled nuclear targeting from catalytic activity, disrupting the former while preserving the latter. This allowed us to specifically test whether IR-induced nuclear import of active IRAK1 is relevant to IR-induced IRAK1 signaling.

In genetic complementation assays performed in vitro and in vivo, we found that IRAK1^{R4A} behaved as a function-null allele. Reconstituting *IRAK1*$^{-/-}$ HeLa cells or Irak1-depleted zebrafish embryos with human IRAK1^{R4A} failed to rescue cell survival in response to IR, affording no added protection as compared to IRAK1^{KD} (Fig. 4, E–H). Furthermore, whereas WT IRAK1 was sufficient to protect radiosensitive Daoy cells from IR-induced cell death, IRAK1^{R4A} failed to do so, yet again mimicking IRAK1^{KD} (Fig. 4, I and J). These experiments showed that nuclear translocation of active IRAK1 is essential for IR-induced IRAK1 signaling.

Nuclear IRAK1 binds PIDD1 and interferes with ATM-induced PIDDosome assembly

We next investigated the significance of IRAK1 nuclear import to IR-induced IRAK1 signaling. The proapoptotic PIDDosome (PIDD1-RAIDD-caspase-2) (31, 34) is a downstream target of IR-induced IRAK1 signaling; PIDDosome inhibition by the kinase accounts, at least in part, for the pathway's prosurvival function (30). PIDDosome assembly has been reported to occur primarily in nucleoli (35), that is, the destination of fully active IRAK1 in irradiated cells (see Fig. 3). Thus, we hypothesized that nuclear entry of active IRAK1 serves, at least in part, to enable PIDDosome inhibition by the kinase. To test this, we used the caspase-2 (C2) bimolecular fluorescence complementation (C2 BiFC) reporter system (36), which probes PIDDosome formation in intact HeLa cells (fig. S4E). As expected from a previous study (30), depletion or inhibition of IRAK1 led to C2 BiFC in irradiated cells in a *PIDD1* and *RAIDD*-dependent manner (fig. S4F), resulting in C2 cleavage and, ultimately, caspase-3 processing (Fig. 4K and fig. S4, G and H). Whereas co-transfections with WT IRAK1 restored PIDDosome inhibition, IRAK1^{R4A} failed to do so and afforded no added protection as compared to IRAK1^{KD} or IRAK1 variants deprived of

activation (T209A) or full activity (T387A) (Fig. 4, L and M). Thus, nuclear translocation of active IRAK1 is an essential feature of non-canonical IRAK1 signaling, critically required for the pathway's anti-apoptotic function via PIDDosome inhibition.

RNAi studies suggested that IRAK1 might block PIDDosome formation by antagonizing ATM-mediated phosphorylation of PIDD1 on Thr^{788} within the death domain (DD) (30), an event necessary for RAIDD recruitment to PIDD1 (37). This role was validated in *IRAK1*$^{-/-}$ HeLa cells (Fig. 4N). Loss of IRAK1 did not otherwise enhance overall ATM activity, per Chk2-$pThr^{68}$ (Fig. 4N), indicating a specific role in the regulation of ATM-mediated PIDD1 phosphorylation.

Like PIDD1, IRAK1 is a DD-containing protein; thus, we explored whether it might act directly by binding PIDD1, possibly through a homotypic DD-DD interaction. Indeed, IRAK1 associated with PIDD1 from approximately 3 to 6 hours after IR until at least 24 hours after stimulus, and the PIDD1 DD was sufficient for the interaction (Fig. 4, O and P). Each of the R4A, T209A, and T387A mutations blocked the ability of IRAK1 to bind PIDD1, indicating that the interaction requires the nuclear translocation and full activation of the kinase (Fig. 4Q). Both the timing of the interaction and the requirement for Thr^{387} phosphorylation were consistent with the accumulation of IRAK1-$pThr^{387}$ in the nucleolus (Fig. 3L). In line with IRAK1 acting to prevent ATM-mediated PIDD1 phosphorylation, removal of IRAK1 extended the ATM-PIDD1 interaction for at least three additional hours (Fig. 4R). Conversely, increasing levels of FLAG-IRAK1 displaced ATM from PIDD1, correlating with a gradual decline in PIDD-$pThr^{788}$ levels (Fig. 4S). The selective IRAK1 inhibitor pacritinib (fig. S4I) (38–40), which was added 3 hours after irradiation to spare early IRAK1 autophosphorylation on Thr^{387} (Fig. 3), failed to block ATM displacement from PIDD1, suggesting that IRAK1 acts non-catalytically (Fig. 4S). Lastly, whereas IRAK1 antagonized ATM-mediated PIDD1 phosphorylation to prevent proapoptotic PIDDosome formation, it had no effect on the formation of prosurvival PIDDosomes in which PIDD1 mobilizes RIP1 in place of RAIDD to stimulate NF-κB (Fig. 4T and fig. S4J) (37, 41–43). Activated IRAK1 also failed to bind TRAF6 after IR, in contrast with IL-1β (Fig. 4U). Together with previous observations that IR-induced phosphorylation of IκBα does not require IRAK1 (30), these results further argue against a role for NF-κB in IR-induced IRAK1 signaling. Collectively, these observations showed that IRAK1 prevents IR-induced cell death by specifically interfering with pro-apoptotic PIDDosome formation.

IR-induced IRAK1 signaling is triggered by DNA damage

Having identified a MyD88-independent, IRAK4-IRAK1 axis activated by IR, we sought to identify the upstream factors which initiate the pathway in place of the pathogen-sensing TLR/IL-1R–MyD88 module.

Even though all known TLR–IL-1R pathways which signal through IRAK1 or IRAK4 do so via MyD88, we first addressed the possibility that a TLR–IL-1R might nevertheless be responsible for IR-induced IRAK1 activation. Indeed, pathways have been identified through which TLRs can signal independently of MyD88 (9, 12). Though none so far have been shown to involve IRAKs, this could be the first instance of such a pathway. Secondly,

irradiated cells may activate paracrine (and conceivably autocrine) TLR–IL-1R signaling via the release of (i) cytokines, PAMPs and DAMPs into the extracellular space which, in turn, might activate cell surface receptors; and, (ii) nucleic acids into the cytoplasm, which may activate intracellular TLRs (44–46). However, medium transfer experiments in which non-irradiated HeLa cells were exposed to supernatant from irradiated donors ruled out an involvement of extracellular factors and cell-surface receptors (Fig. 5, A–C). Similarly, depletion of all known intracellular TLRs—TLR3, TLR7, TLR8 and TLR9—failed to affect IR-induced IRAK1 activation (fig. S5, A–D).

In contrast, multiple independent lines of evidence pointed to IR-induced double strand DNA breaks (DSBs) as responsible for initiating the pathway. First, we had noted that the cytoplasmic activation and nuclear import of IRAK1 correlated with the presence of DNA damage in irradiated nuclei, with nuclear IRAK1-pThr^{209} signals declining coincident with DSB repair (12-24 hpIR) (fig. S2, F and G). Second, drugs which, unlike IR, induce DSBs without causing the release of TLR agonists, such as the radiomimetic bleomycin and the topoisomerase inhibitors camptothecin and topotecan, were sufficient to trigger IRAK1 activation and its transport to the nucleus (fig. S5, E–I). Notably, short incubation with the DNA replication inhibitor aphidicolin, which failed to induce DSBs within the time window we analyzed and induced lower levels of ATR activation compared to that induced by DSBs, had no detectable effect on IRAK1 activation (fig. S5, G and H). In turn, IRAK1 was required for the survival of the damaged cells, similar to its pro-survival role in irradiated cells (Fig. 5D), where again aphidicolin had no effect. Third, in these experiments, the numbers and intensity of nuclear IRAK1-pThr2^{09} foci strictly correlated with the occurrence and extent of DNA damage, whether at a specific time point or as a function of time after stimulus (Fig. 5, E–H, and fig. S5, E–G). In fact, a majority of nuclear IRAK1-pThr^{209} foci overlapped with sites of DNA damage (γH2A.X foci; Fig. 5, E, I and J, and fig. S5, E–G) or with DsRed-PCNA and RFP-Ku70 tracks or foci induced by 2-photon laser micro-irradiation (Fig. 5K and fig. S5J). The strict correlation between DSB levels and IRAK1-pThr^{209} signal intensity was also seen in IR dose responses (fig. S5K), and longer incubations in aphidicolin eventually led to the simultaneous occurrence of DSBs and IRAK1-pThr^{209} foci (fig. S5L). Finally, interrogating the major DSB-sensing kinases (ATM, ATR and DNAPK) (47) identified a requirement for ATR in IR-induced IRAK1 signaling. This was first seen pharmacologically, whereby inhibition of ATR (with ETP46464 and BAY1895344, “ATRi” (48, 49); fig. S5N), but not inhibition of either ATM or DNAPKcs (with KU55933 and NU7441, respectively), blocked IR-induced IRAK1 activation in multiple cell lines (Fig. 5, L and M, and fig. S5M). These results were confirmed using RNAi (Fig. 5, N and P). ATRi, but not ATMi or DNAPKi, also led to PIDDosome activation in irradiated HeLa cells (fig. S5O), as again confirmed genetically (fig. S5P). Collectively, these experiments identified DNA damage as the trigger of IR-induced IRAK1 signaling. Thus, the pathway differs from TLR–IL-1R signaling at the biological, molecular, and subcellular levels, consistent with a non-canonical IRAK signaling pathway.

E3 ubiquitin ligases Pellino1 and Pellino2 exert essential but distinct roles in IR-induced IRAK1 signaling

We next sought to gain first insight into the mechanism by which DNA damage induces IRAK4/1 activation independently of MyD88. The initiating step in the IRAK4-IRAK1 activation cascade, IRAK4 activation via *trans*-autophosphorylation (see Fig. 1), requires proximity-induced dimerization (23–25). Therefore, we reasoned that an adaptor or scaffold molecule would likely be required to enable IRAK4 dimerization in place of MyD88. A previously proposed substitute for MyD88, Unc5CL (50), was dismissed because it showed no RNAi phenotype in human cells (fig. S6, A and B) and is not conserved in zebrafish. We thus focused on other physical interactors of IRAK4 and IRAK1.

The E3 ubiquitin ligases Pellino1 (Peli1), Pellino2 (Peli2) and Pellino3 (Peli3) are homologs of *Drosophila* pellino, a protein originally identified as a physical interactor of the fly IRAK homolog, pelle (51). Human Peli proteins physically and functionally interact with IRAK1 in vitro, acting both as substrates of, and ubiquitin ligases for, IRAK1 (52, 53). We focused on Peli1 and Peli2 because *PELI3*$^{-/-}$ cells could not be recovered despite multiple editing attempts.

PELI1$^{-/-}$ and *PELI2*$^{-/-}$ HeLa cells exhibited striking and distinct phenotypes. Ablation of Peli1 abrogated IR-induced IRAK1 activation altogether, whereas loss of Peli2 had no effect on activation but blocked the nuclear translocation of the activated kinase, trapping it in the cytoplasm (Fig. 6, A and B). In contrast, neither knockout had any discernable effect on IL-1β-induced IRAK1 activation (Fig. 6, A and B). The IR-specific phenotypes, which were confirmed by RNAi in multiple cell lines (fig. S6C), were rescued with respective GFP-tagged full-length proteins (Fig. 6C). GFP-Peli1 failed to rescue *PELI2*$^{-/-}$ cells, and vice versa, confirming the non-redundant roles of either E3 ligase in IR-induced IRAK1 signaling (Fig. 6C).

Although Peli1 and Peli2 exerted distinct functions, loss of either ligase ultimately resulted in the same outcome: loss of nuclear accumulation of IRAK1-pThr^{209}. Consistent with this, *PELI1*$^{-/-}$ and *PELI2*$^{-/-}$ cells both exhibited: (i) a complete loss of fully active IRAK1-pThr^{387} in irradiated nuclei (Fig. 6, D–F); and (ii) marked radiosensitive phenotypes, as evidenced by PIDDosome-mediated C2 activation (Fig. 6, G and H), downstream executioner caspase activation (Fig. 6I and fig. S6D), and reduced overall survival (Fig. 6J) after IR. These phenotypes were recapitulated in *peli1b* and *peli2* morphant zebrafish (Fig. 6, K–N and fig. S6, E–G). Thus, Peli1 and Peli2 are essential for IR-induced IRAK1 signaling, exerting non-redundant roles in the pathway.

Pellino1 associates with IRAK4 and IRAK1 and acts non-catalytically to enable their activation after IR

Finally, we sought to investigate the mechanisms by which Peli1 and Peli2 promote the activation and nuclear transport of IRAK1, respectively. We focused on Peli1 because (i) Peli1, but not Peli2, physically associated with IRAK1 after IR (fig. S7, A and B); and, (ii) none of the currently available anti-Peli2 antibodies specifically recognized Peli2,

precluding biochemical studies at the endogenous level (see Methods). In contrast, the commonly used “Peli1/2” antibody specifically recognized Peli1 (fig. S7C).

To investigate Peli1, we first used a series of deletion- and catalytically-inactive GFP-Peli1 constructs (Fig. 7, A and B) (54). As expected from previous studies (52, 55), GFP-Peli1 interacted with IRAK1 via the N-terminal forkhead-associated (FHA) domain (fig. S7D, note that GFP-Peli1^{C} is the sole construct that fails to interact with IRAK1). The FHA domain was essential for Peli1-mediated IRAK1 activation after IR (Fig. 7, C and D; note the lack of IRAK1-phrT^{209} signal in *PELI1*$^{-/-}$ cells reconstituted with GFP-Peli1^{C}). In contrast, the catalytic RING-like domain was dispensable for Peli1 function (Fig. 7, C and D; note the rescue of *PELI1*$^{-/-}$ cells by GFP-Peli1$^{\Delta C}$). Likewise, each of three catalytically inactive Peli1 variants—H313A, H336A (54) and H369S/C371S (56)—all restored IR-induced IRAK1 activation in *PELI1*$^{-/-}$ cells (Fig. 7, C and D). These observations indicated that Peli1 enables IR-induced IRAK1 activation through its interaction with, but not ubiquitination of, IRAK1.

The structural role played by Peli1 suggested It might enable the IRAK4-IRAK1 interaction itself. Indeed, Peli1 was essential for this event whereas deletion of *PELI2* had no effect (Fig. 7E). Peli1 associated with IRAK4 and IRAK1 as early as 1 min and 5 min after IR, respectively (Fig. 7F). This was in contrast to IL-1β-treated cells, in which Peli1 solely interacted with IRAK1 (active form) but not IRAK4, an observation in line with Peli1 serving as a substrate of IRAK1 in this context (53). IR-induced Peli1/IRAK4/IRAK1 complex formation did not require MyD88, in contrast to the IL-1β–induced Peli1-IRAK1-pThr^{209} interaction (Fig. 7G). These results obtained through Peli1 pulldowns were confirmed in IRAK1pThr^{209} immunoprecipitates (Fig. 7G, middle blots). As expected, IR-induced assembly of the Peli1/IRAK4/IRAK1 platform required ATR (fig. S7E). Thus, after IR, Peli1 associates with both IRAK4 and IRAK1 and functions non-catalytically to promote their interaction and subsequent IRAK1 activation.

These Peli1 properties were reminiscent of that of MyD88 in the TLR/IL-1R pathway, suggesting that Peli1 might act as the adaptor/scaffold (or subunit thereof) which substitutes for MyD88 in the DNA damage-induced pathway. In the immune pathway, MyD88 nucleates the MyDDosome by enabling the dimerization of IRAK4, which when autophosphorylated recruits, phosphorylates and activates IRAK1 (23). Therefore, should Peli1 function as the adaptor in the DSB-induced pathway, we would expect: (i) IRAK4 to be recruited to Peli1 prior to IRAK1; (ii) IRAK1 to be recruited to Peli1 by IRAK4; (iii) Peli1 to be required for the activation of IRAK4 in addition to that of IRAK1; and (iv) IRAK1 recruitment to Peli1 to require IRAK4 catalytic activity. We found all four predictions to be true. First, Peli1 associated with IRAK4 as early as 1 min post-IR, whereas IRAK1 was first detected in the complex at 5 min (Fig. 7F). We also noted that IRAK4 autophosphorylation within the Peli1/IRAK complex initiates earlier than IRAK1 recruitment to the platform (Fig. 7F). This observation was consistent with structural models implicating IRAK4 activation as a prerequisite for the IRAK4-IRAK1 interaction (23). Second, whereas IRAK1 was not required for the Peli1-IRAK4 interaction, IRAK4 was indispensable for IRAK1 recruitment to Peli1 (Fig. 7H). Thus, Peli1 indeed associates with IRAK1 via IRAK4. Third, IR-induced IRAK4 autophosphorylation on Thr^{345}/Ser^{346}

was completely dependent on Peli1 (Fig. 7I), as further verified by western blotting (Fig. 7J). Fourth, despite associating with Peli1 as efficiently as WT IRAK4, kinase-deficient IRAK4 (D329A) failed to mobilize IRAK1 to the complex (Fig. 7K). Collectively, these data identified Peli1 as a critical component of the MyD88-independent platform responsible for IRAK1/4 activation in irradiated cells (Fig. 8).

Discussion

Here, we describe the backbone of a non-canonical pathway of IRAK kinase signaling distinct from the TLR/IL-1R axis. Whereas both pathways share a common mechanism for IRAK1 activation by IRAK4, non-canonical signaling differs upstream and downstream of this core module (Fig. 8). The pathway opens IRAK kinase biology beyond innate immunity and defines unforeseen targets in radio- and chemo-resistant cancers.

IRAK1 catalytic activity is largely dispensable for TLR/IL-1R signaling (57–60), with the kinase instead acting structurally to activate TRAF6 and other effectors (6). Yet in contrast with two of four IRAK family members, the pseudokinases IRAK2 and IRAK3, IRAK1 evolved to retain an intact catalytic domain (19, 61, 62). In the absence of a role for IRAK1 outside of innate immunity, the nature of the selective pressure to preserve its enzymatic activity remained elusive. Our discovery of a non-canonical pathway in which the kinase's activity is essential may explain the evolutionary pressure to retain a functional catalytic site. We found that IRAK1 kinase function is, at minimum, required for autophosphorylation on Thr^{387}, an event necessary for downstream anti-apoptotic signaling. Because $IRAK1^{T387A}$ retained residual activity, additional IRAK1 substrates might be identified in the future. These are unlikely to include the downstream target PIDD1 because IRAK1-mediated inhibition of PIDDosome assembly does not appear to require IRAK1 catalytic activity (Fig. 4S).

Our study describes a physiological mechanism through which cells can activate IRAK4 and IRAK1 in a MyD88-independent manner. A 2012 study showed that overexpression of the DD protein UNC5CL could activate NF-κB and JNK signaling in an IRAK1/4-dependent but MyD88-independent manner (50). However, these observations still await genetic validation, and we have ruled out a role for UNC5CL in non-canonical IRAK signaling. Instead, we identified a non-DD-containing but extensively validated IRAK interactor, Peli1, as the likely adaptor substituting for MyD88. This was surprising given that Peli proteins are viewed as effectors of IRAK1, acting both as substrates of, and E3 ubiquitin ligases for, the active kinase (reviewed in (53, 56, 63)). In line with such a downstream role in canonical IRAK signaling but upstream role in non-canonical signaling, removal of Peli1 or Peli2 had no effect on IL-1β-induced IRAK1 activation in experiments where irradiated *PELI1*$^{-/-}$ and *PELI2*$^{-/-}$ cells analyzed in parallel showed profound phenotypes. Furthermore, the E3 ligase activity of Peli1 was irrelevant to its function in IRAK1/4 activation, echoing earlier studies in the Pellino field where Peli1-3 were viewed as scaffolds orchestrating protein interactions in the TLR/IL-1R pathway (64). Our data support a model where Peli1 first associates with IRAK4 to promote its activation, followed by IRAK1 recruitment to the Peli1/IRAK4 complex and its activation by IRAK4 therein. As such, the Peli1/IRAK4/IRAK1 complex would mirror the activity of the MyDDosome (23, 28). Future studies

will determine whether Peli1, like MyD88, acts by enabling the dimerization of IRAK4, or whether it acts as a subunit of a larger complex in which another molecule is responsible for dimerization.

Interestingly, Peli1 has been implicated in the DDR and, notably, appears to localize to DSBs in response to IR (54, 65), where it undergoes ATM-mediated phosphorylation within minutes of treatment (54). In turn, phosphorylated Peli1 ubiquitinates NBS1 to regulate DSB repair. We found that IRAK1pT209 also localizes at DSBs in response to IR with similar timing, which suggested that DSBs might be the site for Peli1-mediated IRAK1 activation in non-canonical signaling. However, this was ruled out by multiple experiments identifying the cytoplasm as the site of IRAK1 activation in irradiated cells, prior to the nuclear import of the activated kinase. Additionally, ATR, not ATM, is the DDR kinase responsible for engaging non-canonical IRAK signaling. Despite these discrepancies, our study adds to that of others to further implicate Peli1 as a DDR effector (54, 65).

How DSBs and ATR in the nucleus direct Peli1/IRAK4/IRAK1 platform assembly in the cytoplasm is the next fundamental question in the field. The requirement for ATR and not other DSB-transducing kinases may indicate an ATR-specific substrate acting as signaling intermediate. Acute replication stress failed to engage the pathway and correlated with reduced ATR activation compared to that induced by DSBs. That IRAK1 activation might require a minimal threshold of ATR activity may ensure that cells engage non-canonical IRAK1 signaling only in response to severe DNA damage.

Although we could tie the nucleolar localization of IRAK1 to its action as a PIDDosome inhibitor, the significance of its localization at DSBs remains to be explored. Given the pro-survival role of the pathway, a function in DSB repair seems plausible. Another outstanding question is how Peli2 enables the transport of activated IRAK1 to the nucleus. In response to DNA damage, hundreds of proteins are promptly transported to the nucleoplasm where they perform essential functions in DNA repair, transcription and replication (66–68). However, how DNA injury is conveyed to or sensed in the cytoplasm and, in turn, how the nuclear import machinery recruits target cargos for transport, all within minutes of stimulus, remain largely unexplored. This applies to p53 and PTEN, whose nuclear internalizations are essential for tumor suppression (69, 70). Because ubiquitination is critical to the import of PTEN (70) and p53 (71–73), we speculate that Peli2-mediated ubiquitination of IRAK1 might be required likewise.

Our previous work implicated IRAK1 as a driver of tumor-intrinsic resistance to radiotherapy, thus identifying the kinase as a therapeutic target in radiation-resistant cancers (30, 74). Here, we identify immunofluorescence markers of radiotherapy-induced IRAK1 signaling that could be used as diagnostic tools to predict IRAK1i efficacy in patient biopsies, as well as new pathway members (IRAK4, Peli1, Peli2, and ATR) which might define additional targets for inhibition. Additionally, our work reveals that tumor cells can also engage non-canonical IRAK1 signaling in response to DSB-inducing genotoxins such as radiomimetics and topoisomerase inhibitors. IRAK1 was notably essential for the survival of cancer cells treated with such drugs, suggesting a broad applicability of IRAK1 inhibitors in treatment-resistant cancers.

Materials and Methods

Cell Culture, Reagents and X-Ray Irradiation

HeLa (cervical, p53-degraded via HPV-E6), CAL27 (HNSCC, TP53 H183L), SAS (HNSCC, TP53 E336*), MCF7 and MDA-MB-231 (breast, TP53 R280K) cell lines were cultured in DMEM medium (Life Technologies) supplemented with 10% Fetal Bovine Serum (FBS) (Sigma- Aldrich) and 1% penicillin–streptomycin (P/S) (Life Technologies). Daoy (radiosensitive MB cell line) cells were cultured in EMEM medium (Life Technologies) supplemented with 10% FBS and 1% P/S. HeLa, CAL27, Daoy cells were obtained from American Type Culture Collection. SAS cells were purchased from Health Science Research Resources Bank. MDA-MB-231 and MCF7 cells were provided by D. Germain. C2.Pro-BiFC cells (Ando et. al. JCB, 2017) were cultured in DMEM medium (Life Technologies) supplemented with 10% FBS and 1% P/S. ETP46464, camptothecin, aphidicolin and bleomycin were purchased from Sigma-Aldrich. KU-55933 was purchased from TOCRIS. Topotecan and Nu7441 were purchased from Selleckchem. Recombinant human IL-1β was from PeproTech (200-01B). For X-ray IR, cells seeded on 10 cm, 6 well or 96-well plates were irradiated at the indicated doses using the Precision X-rad 320 irradiator. The plates were placed on the programmable shelf with the turntable left on. Filter 1 (2mm Al) and Program 5 (platform height of 50 cm from the source, with an offset of 6 cm and a dose rate of 320 kV) were used in all experiments.

CRISPR–Cas9 Gene Editing

Plasmid lentiCRISPR v2 was digested with BsmBI-v2 (New England Biolabs, R0580) according to the manufacturer's recommendations. Briefly, 1 μg of plasmid was digested for 1 hour at 55 °C, then digested plasmid was gel purified using a QIAquick Gel Extraction kit and eluted in water. Single guide RNA (sgRNA) oligonucleotides for cloning were annealed by mixing them in equal 10 μM concentrations with the addition of 1×T4 DNA ligase buffer, then the mixture was incubated at 37 °C for 30 min, then at 95 °C for 5 min and then ramped down to 25 °C at 5 °C min^{-1}. Hybridized oligonucleotides were diluted 1:200 with H_2O. BsmBI-v2 digested lentiCRISPR v2 plasmid (50 ng) was ligated with 1 μM final concentration oligo duplex using T4 Ligase (NEB, M0202) according to the manufacturer's recommendations and incubated overnight at 4 °C. XL-1 blue competent *E. coli* were transformed with 1 μl of ligation reaction according to the manufacturer's protocol (Agilent Technologies, catalogue no. 200249). Single clones were sequence verified using Sanger sequencing. Lentivirus particles containing sgRNA constructs of *IRAK4*, *PELI1*, *PELI2* and *PELI3* were generated by transfecting Phoenix packaging cells with lentiCRISPR v2 containing corresponding sgRNAs (Eurofins Genomics) and a combination of the lentiviral helper plasmids pCMV-dR8.91 and pMD.G at a ratio of 2:1:1, respectively. jetPEI (Polyplus, 101-10N) was used as the transfection ant. After 24 hrs, medium containing viral particles was collected and concentrated using Lenti-X Concentrator according to the manufacturer's protocol (Clontech, 631231). Briefly, 1 volume of Lenti-X Concentrator was mixed with 3 volumes of 0.45-μm filtered viral particle-containing media. The solution was then incubated overnight at 4 °C. The samples were centrifuged at 1,500 × *g* for 45 min at 4 °C, supernatant aspirated and the pellet resuspended in HeLa cell culture media. For infection, 2×10^5 HeLa cells were plated into 6-well plates. The next day, 5 μM polybrene

(Millipore, tr-1003-g) and 200 μl of concentrated viral particles were added per well. The medium was replaced the next day with medium containing 1 μg ml^{-1} puromycin for selection. *IRAK1*$^{-/-}$ HeLa cells were generated and validated previously (Liu et al., 2019). *PELI3*$^{-/-}$ could not be recovered. sgRNA sequences are listed in table S4.

RNAi

siRNA transfections were performed using X-tremeGENE siRNA transfection reagent (Roche) and 20 nM siRNA according to the manufacturer's instructions. Cells were treated with IR (7.5 Gy) or IL1β (0.1 mg/ml) at 48 hrs post-transfection. Cells were harvested for either western blotting, co-immunoprecipitation or Immunofluorescence 15 mins post-treatment unless otherwise described. Previously validated siRNAs were siLACZ (33), siIRAK1, siIRAK4, siMYD88 (30), siATM and siATR (37) (Qiagen). siRNAs targeting Pellino1, Pellino2, UNC5CL, TLR3, TLR4, TLR7, TLR8, TLR9, Importin-a2 and Importin-b1 were purchased from Qiagen. siRNA sequences are listed in table S3.

Plasmids and DNA Transfection into Cultured Mammalian Cells

pVQAd-IRAK4 WT, D329A and R12C, and pcDNA3-flag-IRAK1 WT, T387A, KD, T209A, T209D, DKD and DProST, were generous gifts from Vicky Rao (32), Michael Martin (27), Xiaoxia Li (75) and Jonathan Ashwell (76). IRAK1^{R4A} was generated from pcDNA3-flag-IRAK1^{WT} using a Q5® Site-Directed Mutagenesis Kit (NEB, E0554S) with the primers IRAK1_R4AF 5'-aaagcagcaCCTCCTATGACCCAGGTGTACG-3' and IRAK1_R4AR 5'-ggccgcggcGTGCAGGCAGCAGCAGGC-3', resulting in $R_{503}RAKRR_{508}$ mutated to $A_{503}AAKAA_{508}$. pEGFP-C1-Flag-Peli1 and derived deletion constructs DFHA1, DFHA2, DC, C, and catalytically inactive mutants H313A and H336A were generous gifts from Chang-Woo Lee (54). The H369S/C371S double-mutant, homologous to the catalytically dead Peli2 H371S/C373S variant (77), was generated from pEGFP-C1-Flag-Peli1 by site-directed mutagenesis using primers Peli1-H369C371S-Q5Fw 5'- GAGCTCAGAAAAGACAACTGCCTATTGGTC-3' and Peli1-H369C371S-Q5Rv 5'- ACGCTCCCACACGGGCTAAACGC-3'. Full-length *PELI2* cDNA (NM_021255.3) was amplified by 2 rounds of PCR using Phusion Flash High-Fidelity PCR Master Mix (Thermo Scientific). The first round was performed using a primer pair within the flanking UTRs of *PELI2*, and the second round was a NESTED PCR. Primers were Peli2-5'UTR-Fw 5'-GCTGCTGTTTTGAGCATGCAA-3', Peli2-3'UTR-Rev 5'-ACTGGCCGCCCCGCGCCCCCTT-3', Peli2-XhoI-Fw 5'-ATACTCGAGGCCACCATGTTTTCCCCTGG-3' and Peli2-HindIII-Rev 5'-AAGCTTTCAGTCAATTGGACCTTGGA-3'. Full-length *PELI2* cDNA was cloned in the pGem®-T easy (Promega) according to the manufacturer's instructions, and was subcloned downstream of EGFP into XhoI and HindIII sites of pEGFP-C1-Flag to obtain pEGFP-C1-Flag-Peli2. All primers for site-directed mutagenesis were designed using NEBaseChanger (https://nebasechanger.neb.com) and all targeted mutations were verified by DNA sequencing. Plasmid DNA transfections were performed using X-tremeGENE HP DNA Transfection Reagent (Roche) with a ratio 2:1 according to the manufacturer's instructions. With the exception of pEGFP-C1-Flag-Peli1^{FL} in Figure 7B–D (0.5 mg/mL), all plasmids were transfected at 1 mg/mL. pDsRed-PCNA (derived from pDsRed, Clontech) and pRFP-Ku70 (derived from pRFP-C/N serial, Clontech) expression plasmids were used

in two-photon micro-IR experiments (see below) and were generously provided by Dr. David Chen from the University of Texas Southwestern and Dr. Li Lan from Massachusetts General Hospital, respectively.

Cell Viability Assays

AlamarBlue-based cell viability assays were performed as described (Liu et al., 2019) with several modifications. Cells were seeded into 96-well plates at a density of 400 cells/well. After 16 hours, cells were treated with bleomycin, camptothecin, topotecan and aphidicolin at their indicated doses or 7.5 Gy IR. 3 days post-treatment, cells were incubated with alamarBlue (Thermo Fisher) at a final concentration of 10%. Absorbance was measured at a wavelength of 570 nm with a 600 nm reference wavelength. Relative fluorescence (RFU) was calculated using cell free wells as a control reference and percent survival was calculated compared to DMSO-treated, non-treated controls. Reverse transfections were performed for siRNAs while seeding the cells. cDNA transfections were performed 24 hrs prior to IR treatment.

Clonogenic Assays

Single-cell suspensions were seeded into 6-well plates (50-200 cells/well) and irradiated at indicated doses. After being cultured for 12 days, plates were rinsed with PBS, incubated with fixing solution (75% methanol, 25% acetic acid) and stained by 0.5% crystal violet (Sigma-Aldrich) in methanol for 30 min at room temperature. Colonies consisting of at least 50 cells were scored.

Immunofluorescence and Confocal Microscopy (Tissue Culture)

Cells (1×10^5) were seeded on coverslips in 6-well plates, fixed in 1% paraformaldehyde, permeabilized in 0.25% Triton X-100, blocked in 1% BSA–PBS for 30 mins at 37°c, stained with indicated primary antibodies (for dilutions, see table S2) for 2 hours at 37 °C and secondary antibody (1:200, anti-rabbit, AlexaFluor 488, AlexaFluor 555, AlexaFluor 647 Invitrogen), mounted in Vectashield with 4,6-diamidino-2-phenylindole (DAPI) and sealed with nail polish, as described previously. Images were obtained under a ×63 NA 1.40 oil objective with an inverted confocal microscope (405 nm, 488 nm, 647 nm; SP5, Leica) and acquired using LAS software. For experiments involving WGA staining, cells were stained with WGA at a dilution of 2.5:1000 prior to permeabilization.

Western Blotting and antibodies

Cells seeded at a density of 0.5 $x10^6$ in 10 cm plates were grown to 60–70% confluence. Cells were transfected with indicated siRNAs for 48 hours and cDNAs for 24 hours. For experiments involving Irradiation, cells were treated with 7.5 Gy IR for 15 min post-transfection, harvested and lysed using 1% NP-40 buffer (Boston BioProducts) with protease and phosphatase inhibitors. Lysates (50 – 200 mg) were incubated at 70°C for 10 minutes after adding NuPAGE LDS Sample Buffer (4X) (Life Technologies) and 5% 2-Mercaptoethanol (Sigma Aldrich). Samples were run on a 10% Bis-tris gel (Nupage) at 170V for 1 hour. After electrophoresis, samples were transferred on a nitro-cellulose membrane (Thermo Fisher Scientific) at 94 V for 100 min. Membranes were then blocked

with 5% Bovine serum albumin (BSA, Sigma Aldrich) in TBS with 0.1% Tween and probed with primary antibodies at 4°C overnight. Membranes were then rinsed with TBS-Tween (5x5 min) and probed with specific HRP-linked secondary antibody in 5% milk or BSA (in TBS-Tween) for 1 hr at room temperature. Membranes were washed as described earlier and placed in SuperSignal West Pico Chemiluminescent Substrate or SuperSignal West Dura Extended Duration Substrate (Pierce Biotechnology). The membrane was then developed with photographic film. A full list of antibodies and dilution/fixation protocol information can be found in table S1. The “Peli1/2” (clone F-7) commercialized by Santa Cruz Biotechnology and other companies recognizes Peli1, but not Peli2 (Figure S7C). To our knowledge, no commercial or custom antibody has been reported that specifically detects Peli2, and none of the three antibodies commercialized as specific to Peli2 (see table S1) recognized Peli2 when tested.

Co-Immunoprecipitation

Lysates for immunoprecipitation (IP) were prepared in 1 or 0.1% NP-40 buffer (1 or 0.1% NP-40, 50 mM Tris-HCl [pH 8.0], 150–250 mM NaCl, 5mM EDTA, 1 mM phenylmethylsulfonyl fluoride, protease inhibitors cocktail [Complete Mini, Roche] and phosphatase inhibitor cocktail [PhosSTOP, Roche]). For endogenous IPs, whole-cell lysates (1–5 mg) were mixed with Protein-G magnetic beads (Invitrogen, 20 μl of a 50% slurry) and IRAK1 and Pellino1 (5 mg, 1 ml final volume) for 10 min to 1 hour at room temp on a rotating wheel. Beads were then washed three times with PBS-Tween20 (0.02%), resolved by SDS-PAGE, and probed with primary antibodies detected with the corresponding secondary antibodies or mouse TrueBlot HRP-conjugated secondary antibodies [eBioscience]). For α-Flag or α-GFP IPs, whole-cell lysates (0.15–2 mg) were mixed with 20 μL beads (50% slurry) and mouse α-Flag (M2) antibody (3 mg) or α–GFP (3 mg) in 1% NP-40 buffer (500 mL final volume) for 10 min on a rotating wheel. Beads were then washed three times with PBS-T, resolved by SDS-PAGE and analyzed by western blot.

Caspase-2 Bimolecular Fluorescence Complementation (C2 BiFC) Imaging

Bimolecular fluorescence complementation (BiFC) uses nonfluorescent N- and C-terminal fragments of the yellow fluorescent protein Venus (“split Venus”) that can associate to reform the fluorescent complex when fused to interacting proteins (Shyu et al., 2006). When the C2 prodomain is fused to each half of split Venus, recruitment of C2 to the PIDDosome and the resulting induced proximity leads to enforced association of the two Venus halves, culminating in the C2 BiFC signal (see Figure 4K). Thus, Venus fluorescence acts as a terminal readout for PIDDosome assembly (Bouchier-Hayes et al., 2009). HeLa.C2 Pro-BiFC cells (Ando et al., 2017) harbor a bicistronic construct in which C2 Pro-VC and C2 Pro-VN, separated by the viral 2A self-cleaving peptide, are translated from a single mRNA transcript. This ensures that C2 Pro-VC and C2 Pro-VN are expressed at equal levels. The sensitivity of the endogenous C2 BiFC reporter is sufficient to detect C2 induced proximity in the nucleolus, a major but not unique site for PIDDosome formation (Ando et al., 2017). Parental HeLa.C2 Pro-BiFC cells (0.5 x 10^5 cells) (Ando et al., 2017) were seeded directly on coverslips, transfected with siRNAs for 48 hours and treated with qVD-OPH (20 μM) and IR (10 Gy) and harvested 24 hours post-treatment. For the experiments including overexpression of IRAK1 cDNA, DNA transfections were done 24 hours after

siRNA transfection, treated with qVD-OPH (20 μM) and IR (10 Gy) and harvested 24 hours post-treatment. Cells expressing the BiFC components were identified by fluorescence of the linked mCherry protein in stable cell lines. Venus channel image data was analyzed to determine the cells positive for C2 BiFC. More than 100 cells were counted over three independent experiments.

Two-photon laser micro-irradiation of SV40 MEF

SV40-immortalized MEFs were transfected with 1.5μg of either pDsRed-PCNA or pRFP-Ku70 expression plasmids using Lipofectamine 2000 (Invitrogen) according to the manufacturer's instructions. The next day, ~10^4 transfected cells were seeded into a 35mm glass-bottom dish and treated with 20μM BrdU. Live-cell imaging was performed 24 hours after BrdU treatment on a Nikon Ti Eclipse inverted microscope (Nikon Inc, Tokyo, Japan) equipped with A1 RMP (Nikon Inc) confocal microscope system (Nikon Inc) and Lu-N3 Laser Units (Nikon Inc). Laser micro-irradiation and imaging were conducted via the NIS Element High Content Analysis software (Nikon Inc) using a 800nm 2-photon laser (10μm x 0.5μm rectangular region, energy level ≅ 2800mW). Images of each cell of interest were acquired at 60x magnification immediately before and immediately after micro-irradiation (~2 seconds acquisition time), as well as 5 minutes after micro-irradiation. 15-20 minutes after micro-irradiation, cells were washed twice with ice-cold PBS, and then fixed in 1% paraformaldehyde, 0.25% Triton fixation buffer on ice for at least 30 minutes. The fixation buffer was replaced with PBS and cells were stored in 4°C until processed for IRAK1pT209 IF analysis.

Zebrafish Lines, Maintenance and X-Ray Irradiation

Adult zebrafish were maintained on a 14:10 hour light:dark cycle at 28°C in accordance with the regulations and policies of the Mount Sinai Institutional Animal Care and Use Committee. The study is compliant with all relevant ethical regulations regarding zebrafish research. The progeny of homozygous $p53^{M214K/M214K}$ ($p53^{MK/MK}$) fish were used throughout. M214 is orthologous to human M246, a commonly mutated residue within the mutational hotspot in the p53 DNA binding domain (http://www-p53.iarc.fr/) (78, 79). $p53^{MK/MK}$ embryos demonstrate fully penetrant resistance to IR-induced cell death (33), a phenotype suppressed by genetic or pharmacological targeting of IRAK1 (30). The TILLING-mediated generation of the $p53^{M214K/M214K}$ line, including allele designation, has been described (33, 80). X-ray irradiation of embryo clutches at 18 hours post-fertilization (hpf) was performed using the X-RAD 320 (PXI Precision X-ray, filter 2) at Mount Sinai hospital irradiator CoRE facility.

Micro-injections into zebrafish embryos

Where using synthetic mRNAs, wild-type (and mutant, when indicated) full-length cDNAs for human IRAK1 (hIRAK1), human IRAK4 (hIRAK4), human Peli1 (hPeli1) and human Peli2 (hPeli2) were subcloned from parent mammalian expression vectors (see the section, Plasmids and DNA transfection into cultured human cancer cells) into the zebrafish expression vector pCS2+. All plasmids were linearized by Sac2 single enzyme treatment at 37 °C for 4 hours. Digests were stopped by adding 1/20 volume 0.5 M EDTA, 1/10 volume of 3 M Na acetate and 2 volumes EtOH. Samples were mixed and chilled at −20 °C for

15 min, washed and resuspended in TE buffer. Sense-capped mRNAs were synthesized for injection using the mMESSAGE mMACHINE SP6 kit (Ambion, #AM1340) following the manufacturer's instructions. mRNA concentrations were determined by Nanodrop and RNA gel. Approximately 20 pg of the synthetic human mRNAs were co-injected with MOs to *irak4*, *irak1*, *peli1b* or *peli2* (table S5) depending on the experiment, during the 1- to 2-cell stage. These synthetic mRNAs encoding human proteins lacked the morpholino antisense oligonucleotide (MO)-target sequences on the corresponding zebrafish endogenous mRNAs, ruling out that any phenotypic rescue resulted from MO titration by the co-injected synthetic mRNA.

Where using MOs,– Splice-junction MOs (Gene Tools LLC) to *irak1*, *irak4* and *myd88* have been previously described (30), and MOs targeted to *peli1b* and *peli2* were designed by and obtained from Gene Tools LLC. MOs were resuspended in sterile water to a stock concentration of 1 mM. Approximately 1 nl 0.25-1 mM MO was delivered into one-cell stage zebrafish embryos by microinjection. Synthetic mRNAs were in vitro transcribed from pCS2+ templates using the Ambion mMESSAGE mMACHINE kit according to the manufacturer's instructions, dispensed as 2 ml aliquots, and stored at −80 °C. Synthetic mRNAs were diluted in RNase free water to a final concentration if 25 ng/ml. Approximately 1 nl mRNA was delivered into one-cell stage embryos by microinjection. All micro-injections of MOs or mRNAs were performed with a NARISHIGE IM 300 microinjector as described in detail online (bio-protocol.org/prep1293). MO-mediated gene knockdowns efficiencies were verified in whole-embryo extracts by western blot when possible or by RT-PCR to detect exon-skipping or intron-retention events (for Irak4, Peli2). All MO sequences and *irak4* and *peli2* RT-PCR primers are listed in tables S5 and S6, respectively.

RT-PCR and Protein Extraction from Zebrafish Embryos

Embryonic RNA was isolated from 24-48 hpf embryos (>15 embryos/sample) using a standard Trizol method (250 μL Trizol (Invitrogen), 50 μL $CHCl_3$, 175 μL isopropanol). One microgram of purified RNA was used to generate cDNA using the Invitrogen SuperScript First Strand III RT-PCR kit, with oligo-dT primers. Two micrograms of the cDNA product were loaded on a 1% agarose gel. Pooled embryo protein lysates were harvested as previously described (33) and analyzed by western blot (see Western blotting and Antibodies).

Acridine Orange (AO) Labeling of live embryos.

At 24 hours after IR, live embryos were labelled with acridine orange at 10 mg ml^{-1} in egg water for 20 min, then dechorionated in pronase (2.0 mg ml^{-1} in egg water) for 5 min and rinsed at least three times for 20 min in egg water. Embryos were imaged with a SMZ1500 fluorescent stereomicroscope and NIS-Element software (Nikon) and analyzed with ImageJ as previously described (33).

Whole-mount immunofluorescence imaging

Zebrafish embryos were injected with 25 pg human IRAK1 mRNA at the one cell stage, irradiated at 18 hpf (see Zebrafish Lines and Maintenance) and fixed at 15 min post-IR

in 4% PFA overnight at 4 °C. Embryos were rinsed three times in PBST, dehydrated with 1:2, 2:1 methanol:PBST, then 3 times in methanol, 5 min each, and stored at −20 °C overnight. Embryos were rehydrated with 2:1, 1:2 methanol:PBST, then 3 times PBST, 5 min each. Embryos were permeabilized with proteinase K (10 mg/ml in PBST) for 3 min, quickly washed 3 times with PBST and fixed with 4% PFA for 20 min. After 5 washes in PBST, 5 min each, 400 ml of blocking reagent was added (1% BSA + 10% normal goat serum (NGS, 10000C, invitrogen) in PBST) and embryos were stored at 4 °C overnight. Anti-IRAK1pT209 was added at 1:100 final concentration in blocking reagent and embryos were incubated at 4 °C over 3 nights on a shaker. Embryos were washed 3 times with PBST, blocked again at 4 °C overnight, and secondary antibody was added (1:300) 4 °C overnight. Finally, embryos were washed 5 times with PBST and processed for whole-mount immunohistochemistry. Images were obtained under a 40x oil objective with an inverted confocal microscope (405 nm, 488 nm; SP5, Leica) and acquired using LAS software. The setting of the software was: size 1024X1024, zoomX2, pinhole 1AU, average 4 for AlexaFluor 555 channel and 2 for all other channels, with Z stacks of 1 mm/slice.

Image Analysis

Cytoplasmic/nuclear Intensity quantification was performed using Intensity Ratio Nuclei Cytoplasm Tool (RRID:SCR_018573) URL: https://github.com/MontpellierRessourcesImagerie/imagej_macros_and_scripts/wiki/Intensity-Ratio-Nuclei-Cytoplasm-Tool, installed as a plug-in in FIJI software. Co-localization analyses were performed with Just Another Co-localization Plugin (JaCoP) https://imagej.net/plugins/jacop, downloaded as a plugin for FIJI. Pearson's coefficient was calculated as a co-localization indicator.

Phylogenetic analyses

Multiple sequence alignments were performed using Clustal Omega (https://www.ebi.ac.uk/Tools/msa/clustalo/).

Statistical Analysis

Paired two-tailed Students t-tests were used to determine p-values ($\alpha = 0.05$). The log rank test was used to determine p-values for survival curves. Data in bar graphs are represented as mean ± SD or ± SEM, as indicated in legends, and statistical significance was expressed as follows: *, $P < 0.05$; **, $P < 0.01$; ***, $P < 0.001$; ns, not significant.

Supplementary Material

Refer to Web version on PubMed Central for supplementary material.

Acknowledgements:

We thank Carlos Franco and Diarles Carles for zebrafish care, and Michael Cohen, Vicky Rao, Xiaoxia Li, Jonathan Ashwell and Chang-Woo Lee for critical reagents. Y.L. was supported by a National Cancer Center postdoctoral fellowship award.

Funding:

S.Z. was supported by NIH/NCI RO1CA275184. S.S. was supported by grants from NIH/NIGMS (RO1GM135301), NIH/NCI (R01CA178162), and Pershing Square Sohn Cancer Research Alliance and New York Community Trust.

Data and Materials Availability:

All data needed to evaluate the conclusions in the paper are present in the paper or the Supplementary Materials. Materials created in this work are available upon request to the corresponding author.

References and Notes

1. Gay NJ, Keith FJ, Drosophila Toll and IL-1 receptor. Nature 351, 355–356 (1991). [PubMed: 1851964]
2. Hashimoto C, Hudson KL, Anderson KV, The Toll gene of Drosophila, required for dorsal-ventral embryonic polarity, appears to encode a transmembrane protein. Cell 52, 269–279 (1988). [PubMed: 2449285]
3. Nusslein-Volhard C, The Toll gene in Drosophila pattern formation. Trends Genet 38, 231–245 (2022). [PubMed: 34649739]
4. Shelton CA, Wasserman SA, pelle encodes a protein kinase required to establish dorsoventral polarity in the Drosophila embryo. Cell 72, 515–525 (1993). [PubMed: 8440018]
5. Lemaitre B, Nicolas E, Michaut L, Reichhart JM, Hoffmann JA, The dorsoventral regulatory gene cassette spatzle/Toll/cactus controls the potent antifungal response in Drosophila adults. Cell 86, 973–983 (1996). [PubMed: 8808632]
6. Janssens S, Beyaert R, Functional diversity and regulation of different interleukin-1 receptor-associated kinase (IRAK) family members. Mol Cell 11, 293–302 (2003). [PubMed: 12620219]
7. Cao Z, Henzel WJ, Gao X, IRAK: a kinase associated with the interleukin-1 receptor. Science 271, 1128–1131 (1996). [PubMed: 8599092]
8. Flannery S, Bowie AG, The interleukin-1 receptor-associated kinases: critical regulators of innate immune signalling. Biochem Pharmacol 80, 1981–1991 (2010). [PubMed: 20599782]
9. O'Neill LA, Golenbock D, Bowie AG, The history of Toll-like receptors - redefining innate immunity. Nat Rev Immunol 13, 453–460 (2013). [PubMed: 23681101]
10. Medzhitov R, Preston-Hurlburt P, Janeway CA Jr., A human homologue of the Drosophila Toll protein signals activation of adaptive immunity. Nature 388, 394–397 (1997). [PubMed: 9237759]
11. Kawasaki T, Kawai T, Toll-like receptor signaling pathways. Front Immunol 5, 461 (2014). [PubMed: 25309543]
12. Fitzgerald KA, Kagan JC, Toll-like Receptors and the Control of Immunity. Cell 180, 1044–1066 (2020). [PubMed: 32164908]
13. Lemaitre B, The road to Toll. Nat Rev Immunol 4, 521–527 (2004). [PubMed: 15229471]
14. Lord KA, Hoffman-Liebermann B, Liebermann DA, Nucleotide sequence and expression of a cDNA encoding MyD88, a novel myeloid differentiation primary response gene induced by IL6. Oncogene 5, 1095–1097 (1990). [PubMed: 2374694]
15. Deguine J, Barton GM, MyD88: a central player in innate immune signaling. F1000Prime Rep 6, 97 (2014). [PubMed: 25580251]
16. Wesche H, Henzel WJ, Shillinglaw W, Li S, Cao Z, MyD88: an adapter that recruits IRAK to the IL-1 receptor complex. Immunity 7, 837–847 (1997). [PubMed: 9430229]
17. Burns K et al. , MyD88, an adapter protein involved in interleukin-1 signaling. J Biol Chem 273, 12203–12209 (1998). [PubMed: 9575168]
18. Medzhitov R et al. , MyD88 is an adaptor protein in the hToll/IL-1 receptor family signaling pathways. Mol Cell 2, 253–258 (1998). [PubMed: 9734363]

19. Muzio M, Ni J, Feng P, Dixit VM, IRAK (Pelle) family member IRAK-2 and MyD88 as proximal mediators of IL-1 signaling. Science 278, 1612–1615 (1997). [PubMed: 9374458]
20. Latty SL et al. , Activation of Toll-like receptors nucleates assembly of the MyDDosome signaling hub. Elife 7, (2018).
21. Lin SC, Lo YC, Wu H, Helical assembly in the MyD88-IRAK4-IRAK2 complex in TLR/IL-1R signalling. Nature 465, 885–890 (2010). [PubMed: 20485341]
22. Motshwene PG et al. , An oligomeric signaling platform formed by the Toll-like receptor signal transducers MyD88 and IRAK-4. J Biol Chem 284, 25404–25411 (2009). [PubMed: 19592493]
23. Wang L et al. , Crystal structure of human IRAK1. Proc Natl Acad Sci U S A 114, 13507–13512 (2017). [PubMed: 29208712]
24. Ferrao R et al. , IRAK4 dimerization and trans-autophosphorylation are induced by Myddosome assembly. Mol Cell 55, 891–903 (2014). [PubMed: 25201411]
25. Cushing L et al. , Interleukin 1/Toll-like receptor-induced autophosphorylation activates interleukin 1 receptor-associated kinase 4 and controls cytokine induction in a cell type-specific manner. J Biol Chem 289, 10865–10875 (2014). [PubMed: 24567333]
26. Cheng H et al. , Regulation of IRAK-4 kinase activity via autophosphorylation within its activation loop. Biochem Biophys Res Commun 352, 609–616 (2007). [PubMed: 17141195]
27. Kollewe C et al. , Sequential autophosphorylation steps in the interleukin-1 receptor-associated kinase-1 regulate its availability as an adapter in interleukin-1 signaling. J Biol Chem 279, 5227–5236 (2004). [PubMed: 14625308]
28. Wang Z et al. , Crystal structures of IRAK-4 kinase in complex with inhibitors: a serine/threonine kinase with tyrosine as a gatekeeper. Structure 14, 1835–1844 (2006). [PubMed: 17161373]
29. Vollmer S et al. , The mechanism of activation of IRAK1 and IRAK4 by interleukin-1 and Toll-like receptor agonists. Biochem J 474, 2027–2038 (2017). [PubMed: 28512203]
30. Liu PH et al. , An IRAK1-PIN1 signalling axis drives intrinsic tumour resistance to radiation therapy. Nat Cell Biol 21, 203–213 (2019). [PubMed: 30664786]
31. Tinel A, Tschopp J, The PIDDosome, a protein complex implicated in activation of caspase-2 in response to genotoxic stress. Science 304, 843–846 (2004). [PubMed: 15073321]
32. De S et al. , Mechanism of dysfunction of human variants of the IRAK4 kinase and a role for its kinase activity in interleukin-1 receptor signaling. J Biol Chem 293, 15208–15220 (2018). [PubMed: 30115681]
33. Sidi S et al. , Chk1 suppresses a caspase-2 apoptotic response to DNA damage that bypasses p53, Bcl-2, and caspase-3. Cell 133, 864–877 (2008). [PubMed: 18510930]
34. Sladky V, Schuler F, Fava LL, Villunger A, The resurrection of the PIDDosome - emerging roles in the DNA-damage response and centrosome surveillance. J Cell Sci 130, 3779–3787 (2017). [PubMed: 29142064]
35. Ando K et al. , NPM1 directs PIDDosome-dependent caspase-2 activation in the nucleolus. J Cell Biol 216, 1795–1810 (2017). [PubMed: 28432080]
36. Bouchier-Hayes L et al. , Characterization of cytoplasmic caspase-2 activation by induced proximity. Mol Cell 35, 830–840 (2009). [PubMed: 19782032]
37. Ando K et al. , PIDD Death-Domain Phosphorylation by ATM Controls Prodeath versus Prosurvival PIDDosome Signaling. Mol Cell 47, 681–693 (2012). [PubMed: 22854598]
38. Hosseini MM et al. , Inhibition of interleukin-1 receptor-associated kinase-1 is a therapeutic strategy for acute myeloid leukemia subtypes. Leukemia 32, 2374–2387 (2018). [PubMed: 29743719]
39. Singer JW et al. , Comprehensive kinase profile of pacritinib, a nonmyelosuppressive Janus kinase 2 inhibitor. J Exp Pharmacol 8, 11–19 (2016). [PubMed: 27574472]
40. Singer JW et al. , Inhibition of interleukin-1 receptor-associated kinase 1 (IRAK1) as a therapeutic strategy. Oncotarget 9, 33416–33439 (2018). [PubMed: 30279971]
41. Janssens S, Tinel A, Lippens S, Tschopp J, PIDD mediates NF-kappaB activation in response to DNA damage. Cell 123, 1079–1092 (2005). [PubMed: 16360037]
42. Tinel A et al. , Autoproteolysis of PIDD marks the bifurcation between pro-death caspase-2 and pro-survival NF-kappaB pathway. Embo J 26, 197–208 (2007). [PubMed: 17159900]

43. Bock FJ et al. , Loss of PIDD limits NF-kappaB activation and cytokine production but not cell survival or transformation after DNA damage. Cell Death Differ 20, 546–557 (2013). [PubMed: 23238565]
44. Apetoh L et al. , Toll-like receptor 4-dependent contribution of the immune system to anticancer chemotherapy and radiotherapy. Nat Med 13, 1050–1059 (2007). [PubMed: 17704786]
45. Candeias SM, Testard I, The many interactions between the innate immune system and the response to radiation. Cancer Lett 368, 173–178 (2015). [PubMed: 25681669]
46. Shan YX, Jin SZ, Liu XD, Liu Y, Liu SZ, Ionizing radiation stimulates secretion of pro-inflammatory cytokines: dose-response relationship, mechanisms and implications. Radiat Environ Biophys 46, 21–29 (2007). [PubMed: 17072632]
47. Blackford AN, Jackson SP, ATM ATR, and DNA-PK: The Trinity at the Heart of the DNA Damage Response. Mol Cell 66, 801–817 (2017). [PubMed: 28622525]
48. Lucking U et al. , Damage Incorporated: Discovery of the Potent, Highly Selective, Orally Available ATR Inhibitor BAY 1895344 with Favorable Pharmacokinetic Properties and Promising Efficacy in Monotherapy and in Combination Treatments in Preclinical Tumor Models. J Med Chem 63, 7293–7325 (2020). [PubMed: 32502336]
49. Wengner AM et al. , The Novel ATR Inhibitor BAY 1895344 Is Efficacious as Monotherapy and Combined with DNA Damage-Inducing or Repair-Compromising Therapies in Preclinical Cancer Models. Mol Cancer Ther 19, 26–38 (2020). [PubMed: 31582533]
50. Heinz LX et al. , The death domain-containing protein Unc5CL is a novel MyD88-independent activator of the pro-inflammatory IRAK signaling cascade. Cell Death Differ 19, 722–731 (2012). [PubMed: 22158417]
51. Grosshans J, Schnorrer F, Nusslein-Volhard C, Oligomerisation of Tube and Pelle leads to nuclear localisation of dorsal. Mech Dev 81, 127–138 (1999). [PubMed: 10330490]
52. Moynagh PN, The roles of Pellino E3 ubiquitin ligases in immunity. Nat Rev Immunol 14, 122–131 (2014). [PubMed: 24445667]
53. Zhang E, Li X, The Emerging Roles of Pellino Family in Pattern Recognition Receptor Signaling. Front Immunol 13, 728794 (2022). [PubMed: 35197966]
54. Ha GH et al. , Pellino1 regulates reversible ATM activation via NBS1 ubiquitination at DNA double-strand breaks. Nat Commun 10, 1577 (2019). [PubMed: 30952868]
55. Lin CC, Huoh YS, Schmitz KR, Jensen LE, Ferguson KM, Pellino proteins contain a cryptic FHA domain that mediates interaction with phosphorylated IRAK1. Structure 16, 1806–1816 (2008). [PubMed: 19081057]
56. Schauvliege R, Janssens S, Beyaert R, Pellino proteins are more than scaffold proteins in TLR/IL-1R signalling: a role as novel RING E3-ubiquitin-ligases. FEBS Lett 580, 4697–4702 (2006). [PubMed: 16884718]
57. Knop J, Martin MU, Effects of IL-1 receptor-associated kinase (IRAK) expression on IL-1 signaling are independent of its kinase activity. FEBS Lett 448, 81–85 (1999). [PubMed: 10217414]
58. Li X et al. , Mutant cells that do not respond to interleukin-1 (IL-1) reveal a novel role for IL-1 receptor-associated kinase. Mol Cell Biol 19, 4643–4652 (1999). [PubMed: 10373513]
59. Maschera B, Ray K, Burns K, Volpe F, Overexpression of an enzymically inactive interleukin-1-receptor-associated kinase activates nuclear factor-kappaB. Biochem J 339 (Pt 2), 227–231 (1999). [PubMed: 10191251]
60. Pauls E et al. , Two phases of inflammatory mediator production defined by the study of IRAK2 and IRAK1 knock-in mice. J Immunol 191, 2717–2730 (2013). [PubMed: 23918981]
61. Lange SM, Nelen MI, Cohen P, Kulathu Y, Dimeric Structure of the Pseudokinase IRAK3 Suggests an Allosteric Mechanism for Negative Regulation. Structure 29, 238–251 e234 (2021). [PubMed: 33238146]
62. Wesche H et al. , IRAK-M is a novel member of the Pelle/interleukin-1 receptor-associated kinase (IRAK) family. J Biol Chem 274, 19403–19410 (1999). [PubMed: 10383454]
63. Moynagh PN, The Pellino family: IRAK E3 ligases with emerging roles in innate immune signalling. Trends Immunol 30, 33–42 (2009). [PubMed: 19022706]

64. Schauvliege R, Janssens S, Beyaert R, Pellino proteins: novel players in TLR and IL-1R signalling. J Cell Mol Med 11, 453–461 (2007). [PubMed: 17635639]

65. Dai L et al. , Pellino1 specifically binds to phospho-Thr18 of p53 and is recruited to sites of DNA damage. Biochem Biophys Res Commun 513, 714–720 (2019). [PubMed: 30987826]

66. Bennetzen MV et al. , DNA damage-induced dynamic changes in abundance and cytosol-nuclear translocation of proteins involved in translational processes, metabolism, and autophagy. Cell Cycle 17, 2146–2163 (2018). [PubMed: 30196736]

67. Fabbro M, Henderson BR, Regulation of tumor suppressors by nuclear-cytoplasmic shuttling. Exp Cell Res 282, 59–69 (2003). [PubMed: 12531692]

68. Knudsen NO, Andersen SD, Lutzen A, Nielsen FC, Rasmussen LJ, Nuclear translocation contributes to regulation of DNA excision repair activities. DNA Repair (Amst) 8, 682–689 (2009). [PubMed: 19376751]

69. Marine JC, p53 stabilization: the importance of nuclear import. Cell Death Differ 17, 191–192 (2010). [PubMed: 20062067]

70. Trotman LC et al. , Ubiquitination regulates PTEN nuclear import and tumor suppression. Cell 128, 141–156 (2007). [PubMed: 17218261]

71. Marchenko ND et al. , Stress-mediated nuclear stabilization of p53 is regulated by ubiquitination and importin-alpha3 binding. Cell Death Differ 17, 255–267 (2010). [PubMed: 19927155]

72. Nikolaev AY, Li M, Puskas N, Qin J, Gu W, Parc: a cytoplasmic anchor for p53. Cell 112, 29–40 (2003). [PubMed: 12526791]

73. Yamasaki S et al. , Cytoplasmic destruction of p53 by the endoplasmic reticulum-resident ubiquitin ligase 'Synoviolin'. EMBO J 26, 113–122 (2007). [PubMed: 17170702]

74. Liu PH, Sidi S, Targeting the Innate Immune Kinase IRAK1 in Radioresistant Cancer: Double-Edged Sword or One-Two Punch? Front Oncol 9, 1174 (2019). [PubMed: 31799178]

75. Yao Z et al. , B23 acts as a nucleolar stress sensor and promotes cell survival through its dynamic interaction with hnRNPU and hnRNPA1. Oncogene 29, 1821–1834 (2010). [PubMed: 20101230]

76. Conze DB, Wu CJ, Thomas JA, Landstrom A, Ashwell JD, Lys63-linked polyubiquitination of IRAK-1 is required for interleukin-1 receptor- and toll-like receptor-mediated NF-kappaB activation. Mol Cell Biol 28, 3538–3547 (2008). [PubMed: 18347055]

77. Ordureau A et al. , The IRAK-catalysed activation of the E3 ligase function of Pellino isoforms induces the Lys63-linked polyubiquitination of IRAK1. Biochem J 409, 43–52 (2008). [PubMed: 17997719]

78. Olivier M et al. , The IARC TP53 database: new online mutation analysis and recommendations to users. Hum Mutat 19, 607–614 (2002). [PubMed: 12007217]

79. Olivier M, Hollstein M, Hainaut P, TP53 mutations in human cancers: origins, consequences, and clinical use. Cold Spring Harb Perspect Biol 2, a001008 (2010). [PubMed: 20182602]

80. Berghmans S et al. , tp53 mutant zebrafish develop malignant peripheral nerve sheath tumors. Proc Natl Acad Sci U S A 102, 407–412 (2005). [PubMed: 15630097]

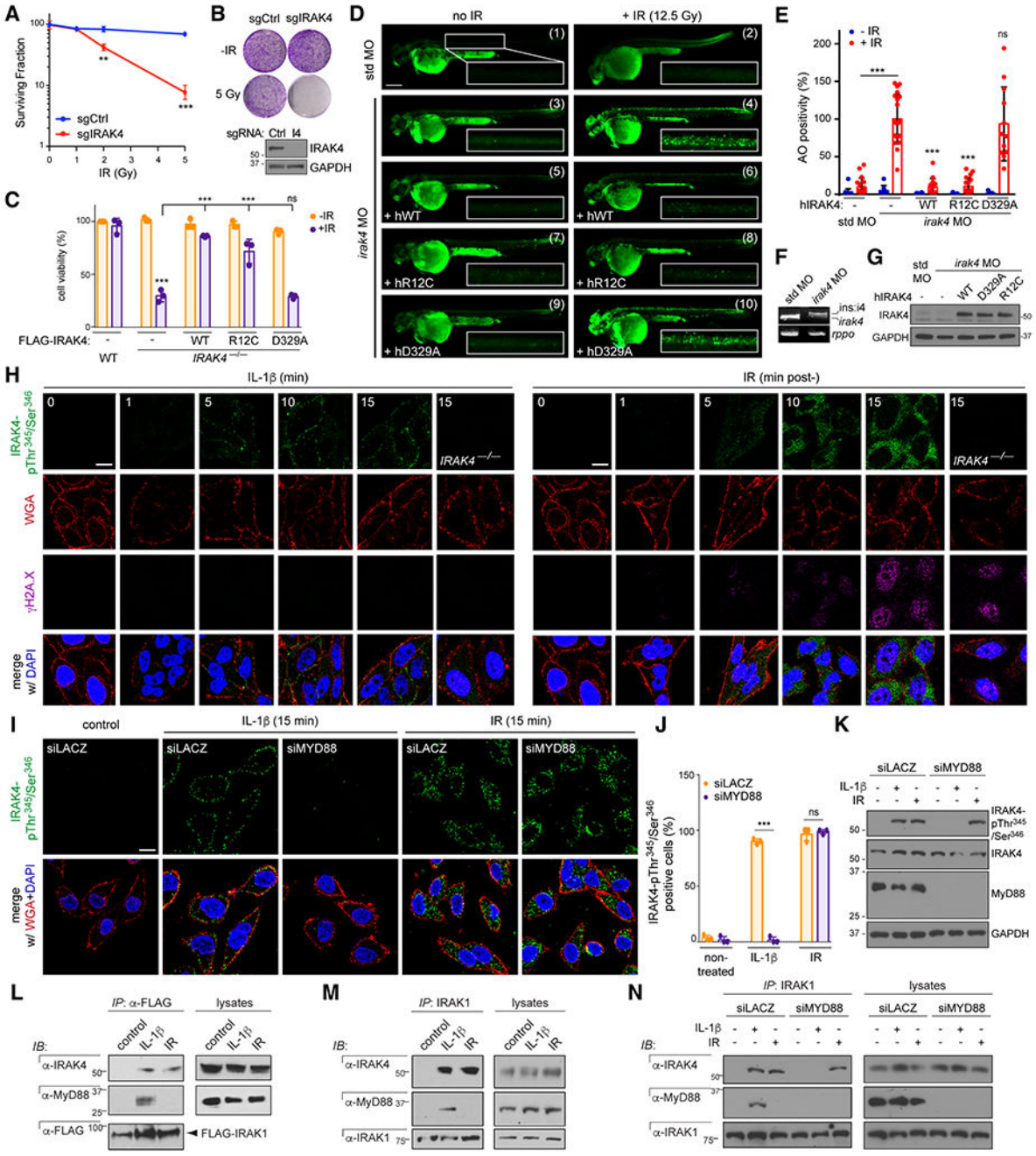

Fig. 1. IRAK4 associates with IRAK1 and is required for cell survival after IR in a MyD88-independent manner.

(**A** and **B**) Parent and *IRAK4*$^{-/-}$ HeLa cells were treated with indicated doses of X-IR (IR) and colonies were counted (A) and imaged (B) at 12 days post-IR. Western blot verifying IRAK4 knockout shown in (B). (**C**) Parent and *IRAK4*$^{-/-}$ cells reconstituted with indicated FLAG-IRAK4 constructs were treated with or without IR (7.5 Gy). Cells were stained with alamarBlue 72 hours after IR. Expression levels of FLAG-IRAK4 variants are shown in fig. S1C. (**D** and **E**) *p53*$^{MK/MK}$ zebrafish embryos were co-injected at the 1-cell stage with the

indicated MOs with or without synthetic mRNAs for the indicated human (h) FLAG-IRAK4 variants. Embryos were treated with or without whole-body IR (12.5 Gy) 18 hours later and stained with acridine orange (AO) at 24 hours after IR to label apoptotic cells in vivo. Spinal cord areas dorsal to the yolk tube (boxed) were quantified (E) from at least $n = 6$ embryos per condition over 3 independent experiments. Data are means ± SEM, $*p < 0.05$, $**p < 0.01$, $***p < 0.001$, two-tailed Student's t-test. Scale bar, 0.2 mm. (**F**) mRNA extracts from embryos injected with indicated MOs were analyzed by RT-PCR. *irak4* MO targets the exon4/intron4 splice junction, resulting in the retention of intron 4 (199 bp), as verified by sequencing. (**G**) Pooled whole-embryo extracts from (D) analyzed by western blot. (**H**) HeLa cells were treated with IL-1β (0.1 μg/mL; left) or IR (7.5 Gy; right), fixed at indicated time points (min), stained with indicated antibodies, and co-stained with membrane marker wheat germ agglutinin (WGA) and nuclear marker DAPI. Confocal images representative of at least 80 cells per condition over $n = 3$ independent experiments. Scale bar, 5 μm. (**I** and **J**) HeLa cells transfected with indicated siRNA were treated with or without IL-1β (0.1 μg/mL) or IR (7.5 Gy) and fixed at 15 min. Confocal images representative of at least 80 cells per condition over $n = 3$ independent experiments (H) were quantified in (I). Single channels shown in fig. S1D. Scale bar, 5 μm. (**K**) Whole-cell lysates from cells in (I) were analyzed by western blot. (**L** and **M**) FLAG-IRAK1-transfected (L) or non-transfected (M) HeLa cells were treated with or without IL-1β (0.1 μg/mL) or IR (7.5 Gy) and lysed at 15 min. FLAG (L) or endogenous IRAK1 (M) immunoprecipitates were analyzed by western blot. *IP*, immunoprecipitate; *IB*, immunoblot. (**N**) HeLa cells transfected with the indicated siRNAs were treated with or without IL-1β (0.1 μg/mL) or IR (7.5 Gy) and lysed at 15 min. IRAK1 immunoprecipitates were analyzed by western blot. All blots (F, K-N) are representative of at least $n = 2$ independent experiments. Data in (A, C and J) are means ± SD of $n = 3$ independent experiments with $**p < 0.01$ and $***p < 0.001$, two-tailed Student's t-test.

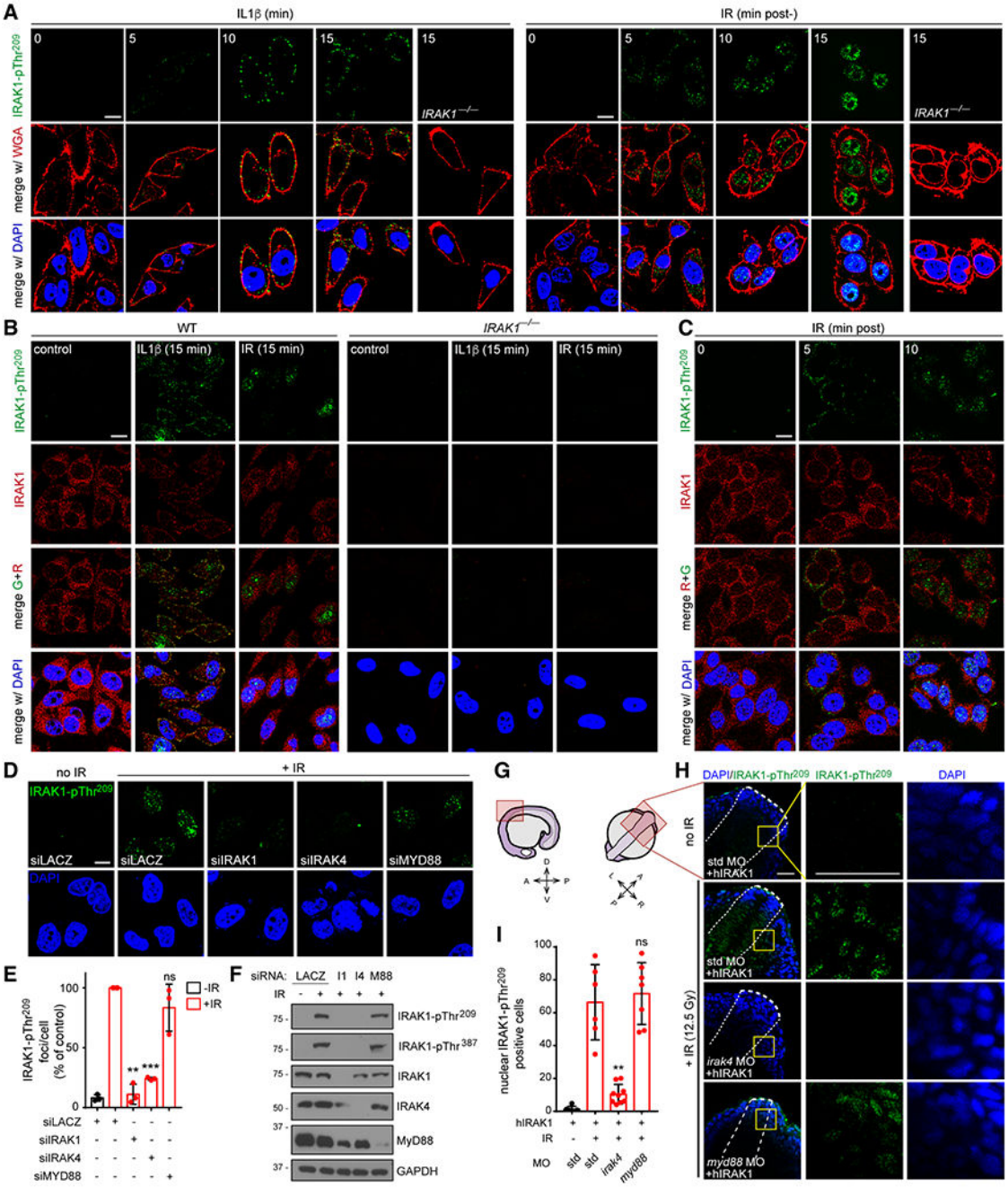

Fig. 2. Active IRAK1 accumulates in the nucleus of irradiated cells in an IRAK4-dependent but MyD88-independent manner

(**A**-**C**) Parental and *IRAK1*$^{-/-}$ HeLa cells were treated with IL-1β (0.1 μg/mL) or IR (7.5 Gy), fixed at indicated time points (min), stained with indicated antibodies and imaged by confocal microscopy. (**D**-**F**) HeLa cells transfected with indicated siRNA were treated with or without IR (7.5 Gy), fixed at 15 min, and stained with IRAK1pThr^{209} antibody (D; quantified in (E)) or analyzed by western blot (F). I1, IRAK1; I4, IRAK4; M88, MYD88. Data in (E) are means ± SD of 3 independent experiments. Statistical significance vs. bar

2: **p<0.01, ***p < 0.001; two-tailed Student's t-test. (**G**) Schematic of lateral and dorsal views of the 18-hour zebrafish embryo, with imaged area (see H) boxed in pink. A, anterior; P, posterior; V, ventral; D, dorsal; L, left; R, right. (**H and I**) *p53*$^{MK/MK}$ embryos were co-injected at the 1-cell stage with the indicated MOs with or without synthetic mRNA encoding human FLAG-IRAK1 (hIRAK1) to detect IRAK1-pThr^{209} in vivo (std, standard control MO). 18 hours later, embryos were (or were not) whole-body exposed to IR (12.5 Gy), fixed 15 min later and stained as whole-mounts with IRAK1-pThr^{209} antibody (which does not cross-react with zebrafish Irak1) and DAPI. Higher-magnification images of the boxed areas shown to the right were used for quantification shown in (I). Anterior and spinal cord areas delineated by thick and thin dashed lines, respectively. Scale bar, 40 μm. (**I**) Quantification of spinal cord areas (such as boxed in (H)) of at least n = 6 embryos per condition over 3 independent experiments. Data are means +/− SEM, statistical significance vs. bar 2: **p < 0.01, two-tailed Student's t-test. Confocal images in (A-D) and blots in (F) representative of n = 3 independent experiments, with at least 80 cells analyzed per condition in (A-D). Scale bars in (A-D), 5 μm.

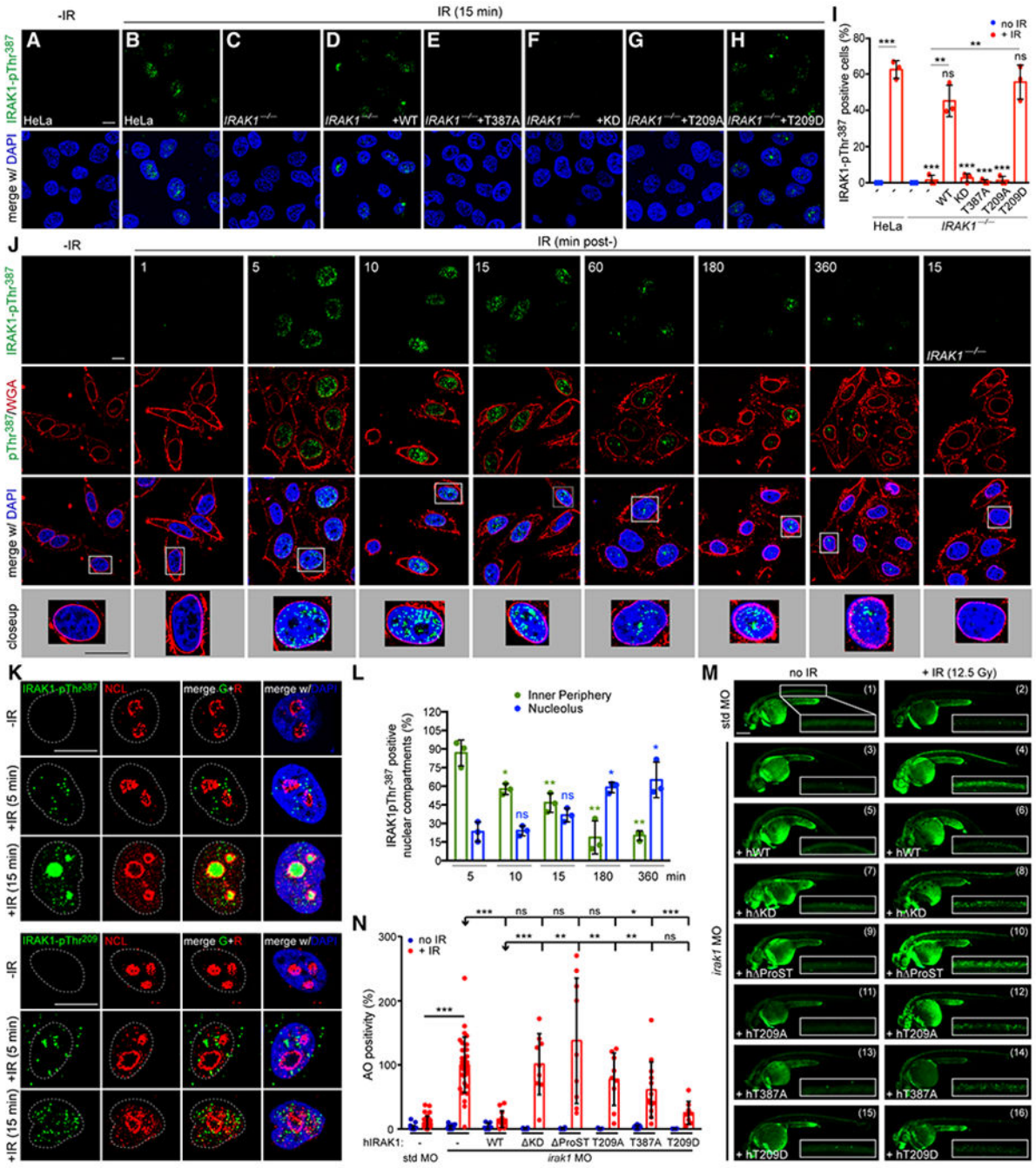

Fig. 3. IRAK1 autophosphorylates in the nucleus of irradiated cells and relocates to nucleoli as a fully active kinase

(**A-H**) *IRAK1*$^{-/-}$ HeLa cells reconstituted with indicated FLAG-IRAK1 constructs were treated ± IR (7.5 Gy), fixed 15 min after and stained with IRAK1-pThr^{387} antibody. (**I**) Quantification of stains such as in (A-H). Data are means ± SD of at least 80 cells analyzed per condition over $n = 3$ independent experiments. $^{**}p < 0.005$, $^{***}p < 0.001$ ns, non-significant, by two-tailed Student's t-test. (**J**) HeLa cells were treated with or without IR (7.5 Gy), fixed at indicated time points (min), stained with IRAK1-pThr^{387} antibody

and co-stained with WGA and DAPI. Higher-magnification images of the boxed areas are also shown. (**K**) HeLa cells treated as above stained with antibodies to nucleolin (NCL) and IRAK1-pThr^{387} (top) and IRAK1-pThr^{209} (bottom). Images are close-ups of boxed areas in fig. S3C. (**L**) Quantification of images as shown in (J). Data are means +/− SD of 3 independent experiments with at least 80 cells analyzed per condition. $^{**}p < 0.05$, $^{**}p < 0.005$, ns, non-significant, by two-tailed Student's t-test. (**M**) Zebrafish *p53*$^{MK/MK}$ embryos were co-injected at the 1 cell stage with the indicated MOs ± synthetic mRNAs for the indicated human FLAG-IRAK1 variants. Embryos were treated with or without whole-body IR (12.5 Gy) 18 hours later and stained with acridine orange (AO) at 24 hours after IR to label apoptotic cells in vivo. Spinal cord areas dorsal to the yolk tube (boxed in each panel) were used for quantification shown in (N). Scale bar, 0.2 mm. (**N**) Quantification of spinal cord areas (such as boxed in (M)) of at least $n = 6$ embryos per condition over at least 3 independent experiments. Data are means +/− SEM. Statistical significance vs. bars 2, 4 or 6: $^{*}p < 0.05$, $^{**}p < 0.01$, $^{***}p < 0.001$, by two-tailed Student's t-test. Confocal images in (A-K) representative of $n = 3$ independent experiments. Scale bars, 10 μm.

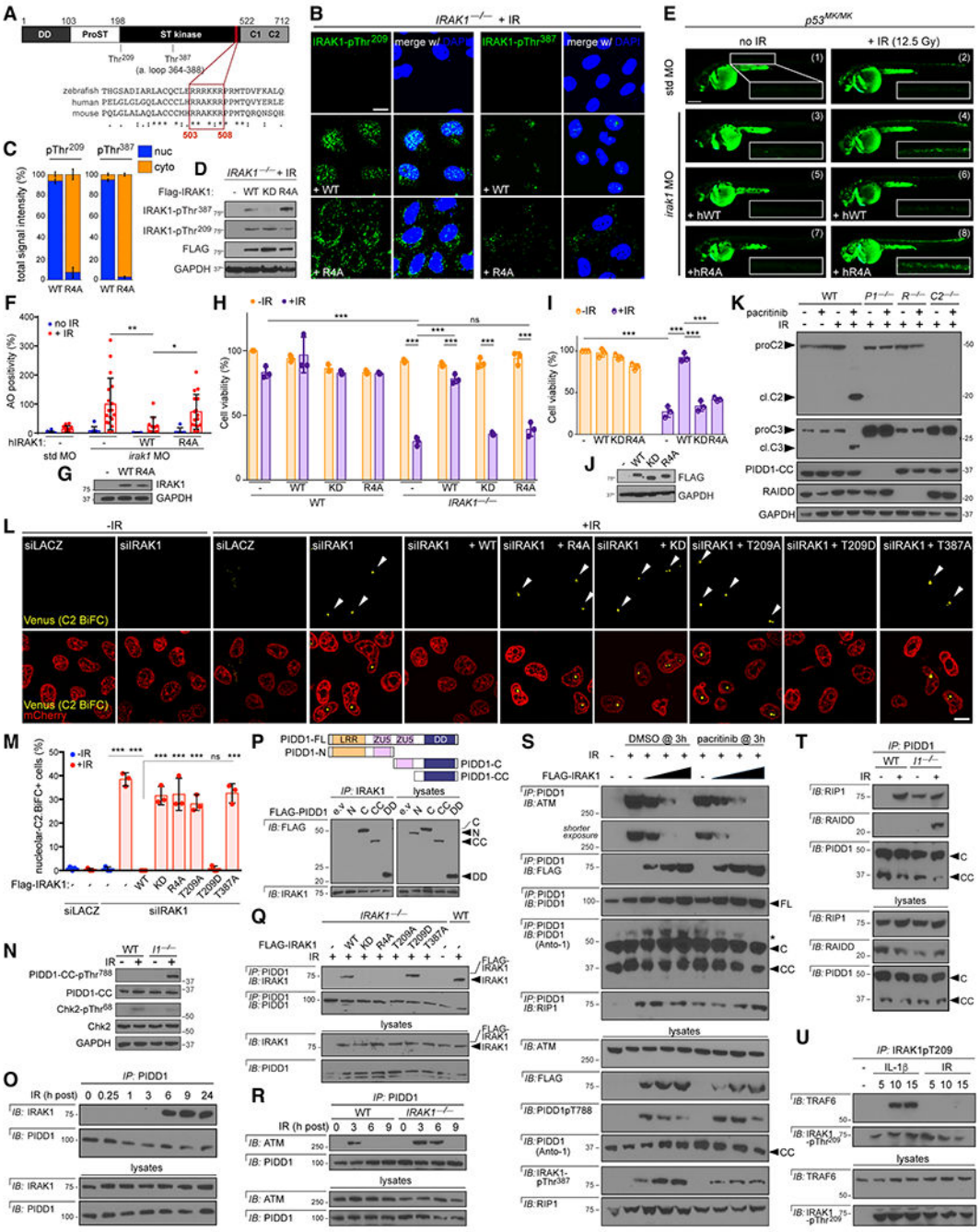

Fig. 4. Nuclear internalization of active IRAK1 enables PIDDosome inhibition and is essential for IR-induced IRAK1 signaling.

(**A**) Identification of a conserved putative NLS, Arg^{503}-RAKR-Arg^{508}, at the distal end of the IRAK1 kinase domain. DD, death domain; ProST, Pro/Ser/Thr -rich domain; ST kinase, Ser/Thr kinase; C1 and C2, C-terminal regions 1 and 2. (**B**) *IRAK1*$^{-/-}$ HeLa cells reconstituted with indicated FLAG-IRAK1 constructs were treated with IR (7.5 Gy), fixed 15 min later, and stained as indicated. Images are representative of at least 80 cells per condition over $n = 3$ independent experiments, quantified in (C). R4A, RRAKRR

→ AAAKAA. See fig. S4C–D for expression levels of FLAG-IRAK1 variants and non-irradiated and parental controls. (**C**) Quantification of signals from $n = 3$ independent experiments such as in (B). (**D**) Cells from (B) were analyzed by western blot. (**E**) Zebrafish $p53^{MK/MK}$ embryos were co-injected at the 1-cell stage with the indicated MOs with or without synthetic mRNAs for the indicated human (h) FLAG-IRAK1 variants. Embryos were treated with or without whole-body IR (12.5 Gy) 18 hours later and stained with acridine orange (AO) at 24 hours after IR to label apoptotic cells. Spinal cord areas dorsal to the yolk tube (boxed in each panel) were used for quantification shown in (F). Scale bar, 0.2 mm. (**F**) Quantification of spinal cord areas (such as boxed in (E)) of at least $n = 6$ embryos per condition over 3 independent experiments, with data expressed as means +/− SEM, $*p < 0.05$, $**p < 0.01$, by two-tailed Student's t-test. (**G**) Pooled whole-embryo extracts from (E-F) analyzed by western blot. The human IRAK1 antibody does not detect endogenous zebrafish Irak1. (**H** and **I**) $IRAK1^{-/-}$ HeLa cells (H) and Daoy cells (I) reconstituted with indicated FLAG-IRAK1 constructs were treated ± IR (7.5 Gy) and stained with the vital dye alamarBlue 72 hours after IR. (**J**) Cells from (I) were lysed and analyzed by western blot. (**K**) SV40 MEF of indicated genotypes were treated with or without IR (7.5 Gy) and IRAK1 inhibitor pacritinib (0.1 μM) (see fig. S4I), harvested at 36 hours after IR and analyzed by western blot. *P1*, *Pidd1*; *R*, *Raidd*; proC2, procaspase-2; cl.C2, cleaved C2 (p19); proC3, procaspase-3; cl.C3, cleaved C3; PIDD1-CC, C-terminal double autocleavage product and subunit of the pro-apoptotic PIDDosome. (**L** and **M**) C2.Pro-BiFC HeLa cells (see fig. S4E–F) were transfected with indicated siRNA ± indicated FLAG-IRAK1 variants, treated with or without IR (10 Gy) and scored for nucleolar C2 BiFC 24 hours after IR. Arrowheads in (L) mark nucleolar C2 BiFC signals. Images representative of at least 80 cells per condition over $n = 3$ independent experiments. (**N to U**) HeLa cells of indicated genotypes (N-O, Q-U)) or stably expressing shPIDD1 (P), transfected with indicated FLAG-tagged constructs (P,Q,S), and treated as indicated with IR (7.5 Gy), IRAK1i pacritinib (pac, 0.1 μM, (S)) or IL-1β (0.1 μg/mL, (U)), were harvested at the indicated time points (O,R,U) or at 24 hours (N, T) or 6 hours (Q, S) after IR, or at 24 hours after transfection (P). Whole-cell lysates were directly analyzed by western blot (N) or immunoprecipitated with the indicated antibodies prior to NU-PAGE analysis (O-U). All blots are representative of at least $n = 2$ independent experiments. Data in (H, I and M) are means ± SD of $n = 3$ independent experiments, and $***p < 0.001$ by two-tailed Student's t-test. Scales bars in (B and L), 5 μm.

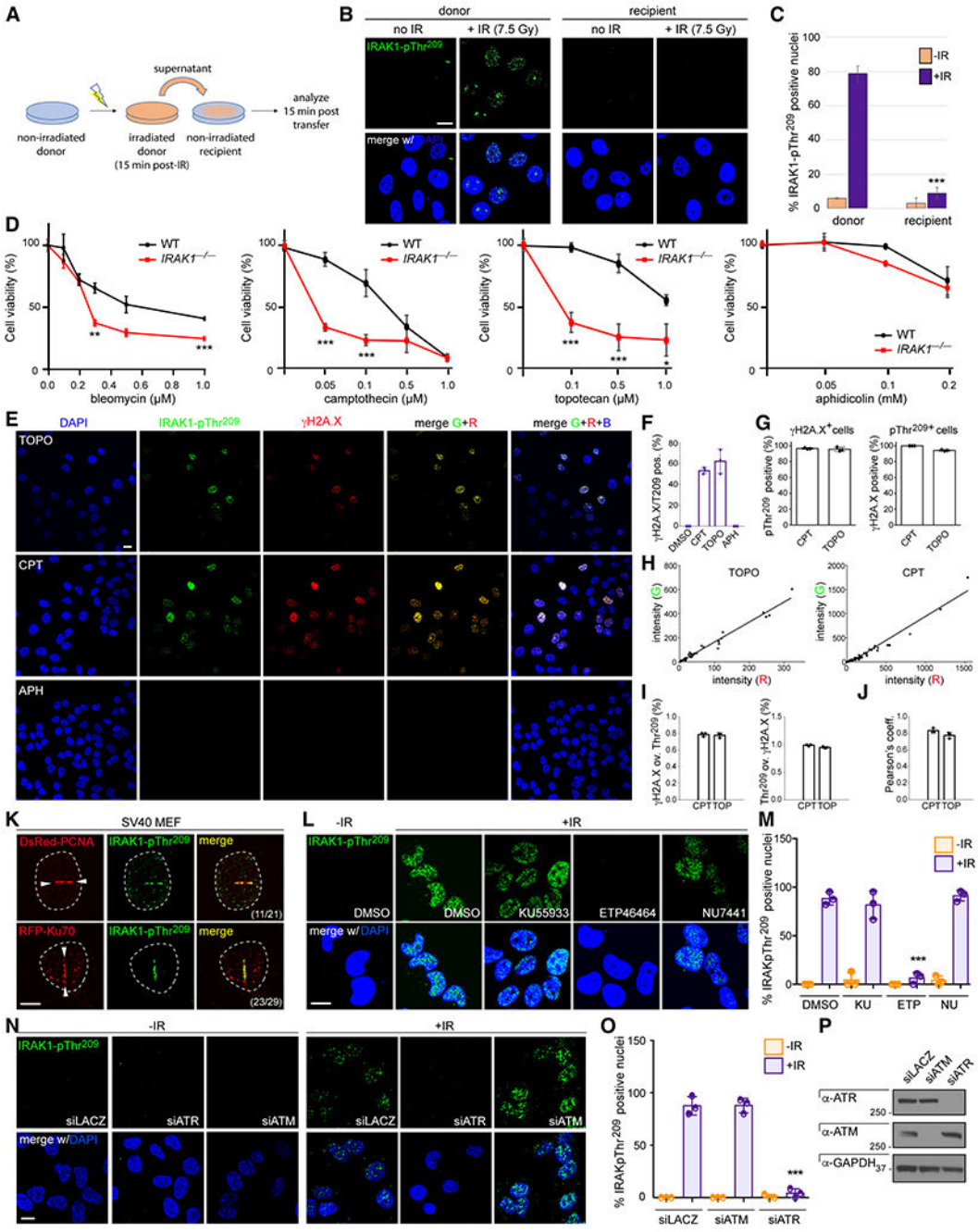

Fig. 5. Non-canonical IRAK1 signaling is a DNA damage response

(**A**) Schematic of the medium-transfer experiments performed. (**B** and **C**) HeLa cells treated as shown in (A) were stained with IRAK1-pThr^{209} antibody and DAPI, imaged by confocal microscopy (B), and quantified (C). (**D**) Parental and *IRAK1*$^{-/-}$ HeLa cells treated with indicated genotoxins were stained with the vital dye alamarBlue 72 hours after treatment. (**E**) HeLa cells treated with the indicated genotoxins were fixed after 6 hours and stained with the indicated antibodies and DAPI. TOPO, topotecan (1 μM); CPT, camptothecin (1 μM); APH, aphidicolin (0.2 mM). See fig. S5E–G for the full time course. (**F**) Cells

double-positive for γH2A.X and IRAK1-pThr^{209} were counted from $n = 3$ independent experiments such as shown in (E). (**G**) The percentages of γH2A.X^{+} cells positive for IRAK1-pThr^{209} (left), and vice versa (right), were counted as above. (**H**) Intensity of IRAK1-pThr^{7209} (G) signals relative to that of γH2A.X (R) in individual cells from (E) after treatment with TOPO (left) or CPT (right). (**I**) Percentages of γH2A.X^{+} foci positive for IRAK1pT209 (left), and vice versa (right), were counted from $n = 3$ independent experiments as in (E). (**J**) Pearson's coefficient derived from image analyses in (I). (**K**) RFP-PCNA (top) and RFP-Ku80 (bottom) -expressing SV40 mouse embryonic fibroblasts (MEF) exposed to two photon laser micro-irradiation were stained with IRAK1-pThr^{209} antibody 15 min after treatment. DNA damage tracks indicated with arrowheads. Number of cells showing staining overlap between IRAK1-pThr^{209} and RFP-PCNA tracks (over $n = 3$ independent experiments) or RFP-Ku80 tracks or foci (over $n = 2$ independent experiments) are indicated. See fig. S5J for RFP-Ku80 foci. (**L**) HeLa cells exposed to the indicated kinase inhibitors were treated with or without IR (7.5 Gy), fixed at 15 min and stained for IRAK1-pThr^{209} antibody and DAPI. KU55933, ATMi (10 μM); ETP46464, ATRi (10 μM); NU7441, DNA-PKi (5 μM). (**M**) Quantification of stains from experiments as in (L). (**N**) HeLa cells transfected with indicated siRNA were treated with or without IR (7.5 Gy), fixed at 15 min and stained for IRAK1-pThr^{209} antibody and DAPI. (**O**) Quantification of IRAK1-pThr^{209} stains from experiments as in (N). (**P**) Whole cell lysates from cells as in (N) were analyzed by western blot. Confocal images in (B, E, L and N) and blots in (P) representative of $n = 3$ independent experiments, and data in (C, D, M and O) reported as means ± SD of 3 independent experiments, $*p < 0.05$, $**p < 0.005$, $***p < 0.001$, two-tailed Student's t-test. Scale bars, 5 μm. Confocal images in (B, E, K, L and N) are representative of at least 80 cells per condition over $n = 3$ independent experiments.

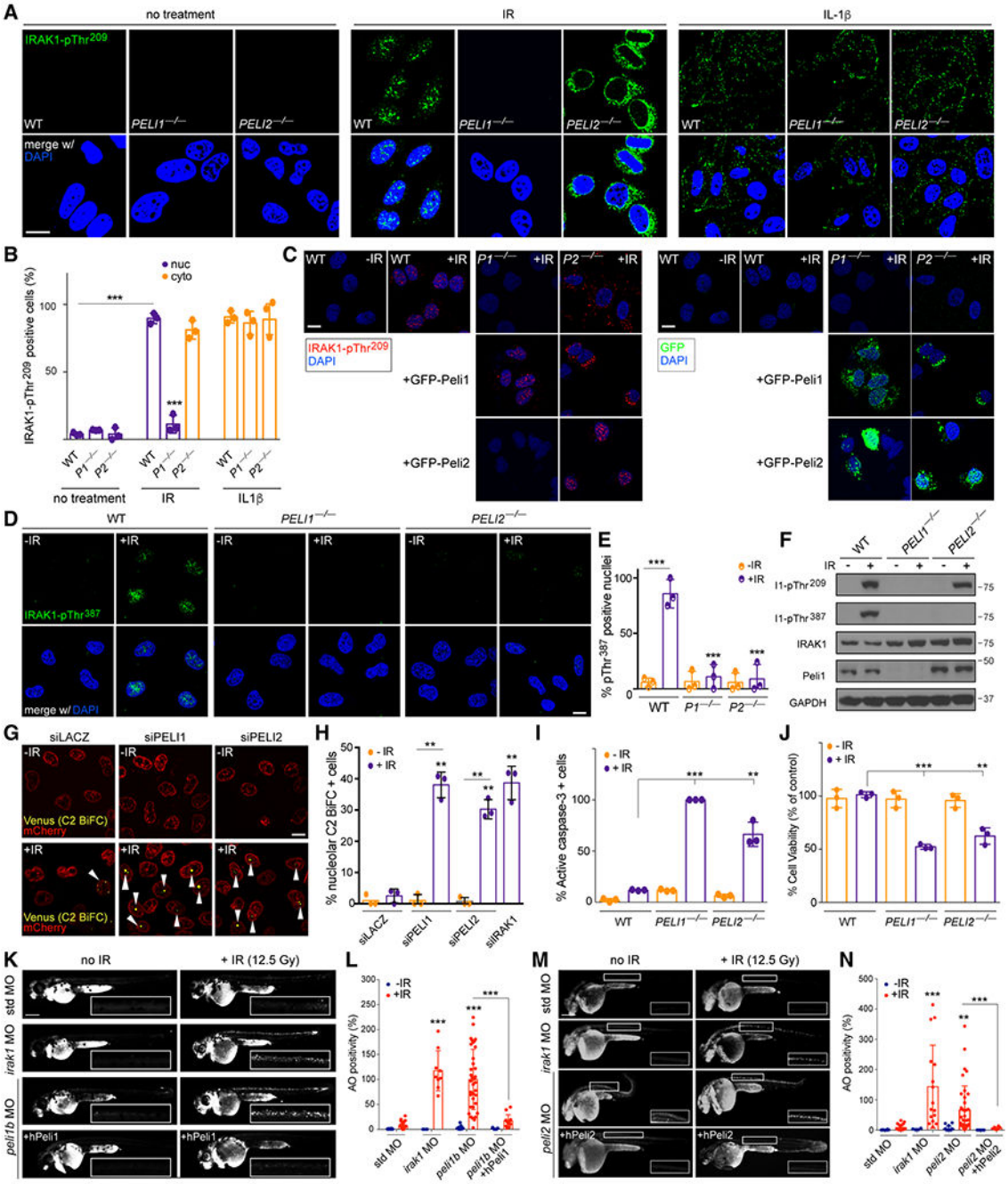

Fig. 6. Essential and distinct roles of Peli1 and Peli2 in non-canonical IRAK1 signaling.

(**A** and **B**) Parent, *PELI1*$^{-/-}$ and *PELI2*$^{-/-}$ HeLa cells were treated with or without IR (7.5 Gy) or IL-1β (0.1 μg/mL), fixed at 15 min, stained as indicated (A), and signals were spatially quantified (B). (**C**) Parent, *PELI1*$^{-/-}$ (*P1*$^{-/-}$) and *PELI2*$^{-/-}$ (*P2*$^{-/-}$) cells reconstituted with indicated GFP-Peli constructs were treated with or without IR (7.5 Gy), fixed at 15 min, stained as indicated and additionally analyzed for GFP (green) by confocal microscopy. (**D** and **E**) Parent, *PELI1*$^{-/-}$ and *PELI2*$^{-/-}$ cells were treated with or without IR (7.5 Gy), fixed at 15 min, stained as indicated (D) and signals were quantified (E).

(**F**) Whole-cell lysates from experiments as in (D) were analyzed by western blot. (**G** and **H**) C2.Pro-BiFC HeLa cells transfected with indicated siRNA were treated ± IR (7.5 Gy) and fixed at 24 hours after IR. Arrowheads mark nucleolar BiFC signals reflective of PIDDosome assembly (G), quantified in (H). (**I**) Parent, *PELI1*$^{-/-}$ and *PELI2*$^{-/-}$ cells were treated ± IR (7.5 Gy), fixed at 48 hours, and stained with antibody to active caspase-3 and DAPI. Representative images are shown in fig. S6D. (**J**) Cells as in (I) were stained with the vital dye alamarBlue 72 hours after IR. (**K-N**) Zebrafish *p53*$^{MK/MK}$ embryos were co-injected at the 1-cell stage with the indicated MOs with or without synthetic mRNA for corresponding human Peli (hPeli) proteins. Embryos were treated with or without whole-body IR (12.5 Gy) 18 hours later and stained with acridine orange (AO) to label apoptotic cells. Spinal cord areas dorsal to the yolk tube (boxed in each panel) were used for quantification, shown in (L and N). Scale bar, 0.2 mm. *peli1b*, zebrafish *PELI1* ortholog, as based on Clustal Omega analysis (fig. S6E). At least $n = 3$ embryos per condition were analyzed in each of at least 2 independent experiments. Data are means +/− SEM, $*p < 0.05$, $**p < 0.01$, $***p < 0.001$, two-tailed Student's t-test. Data in (A, B, D, E, G, H, I and J) are representative of, and presented as means ± SD of, $n = 3$ independent experiments, with confocal images representative of at least 80 cells per condition; $**p < 0.005$; $***p < 0.001$, by two-tailed Student's t-test. Scale bars in (A, C, D and G), 5 μm.

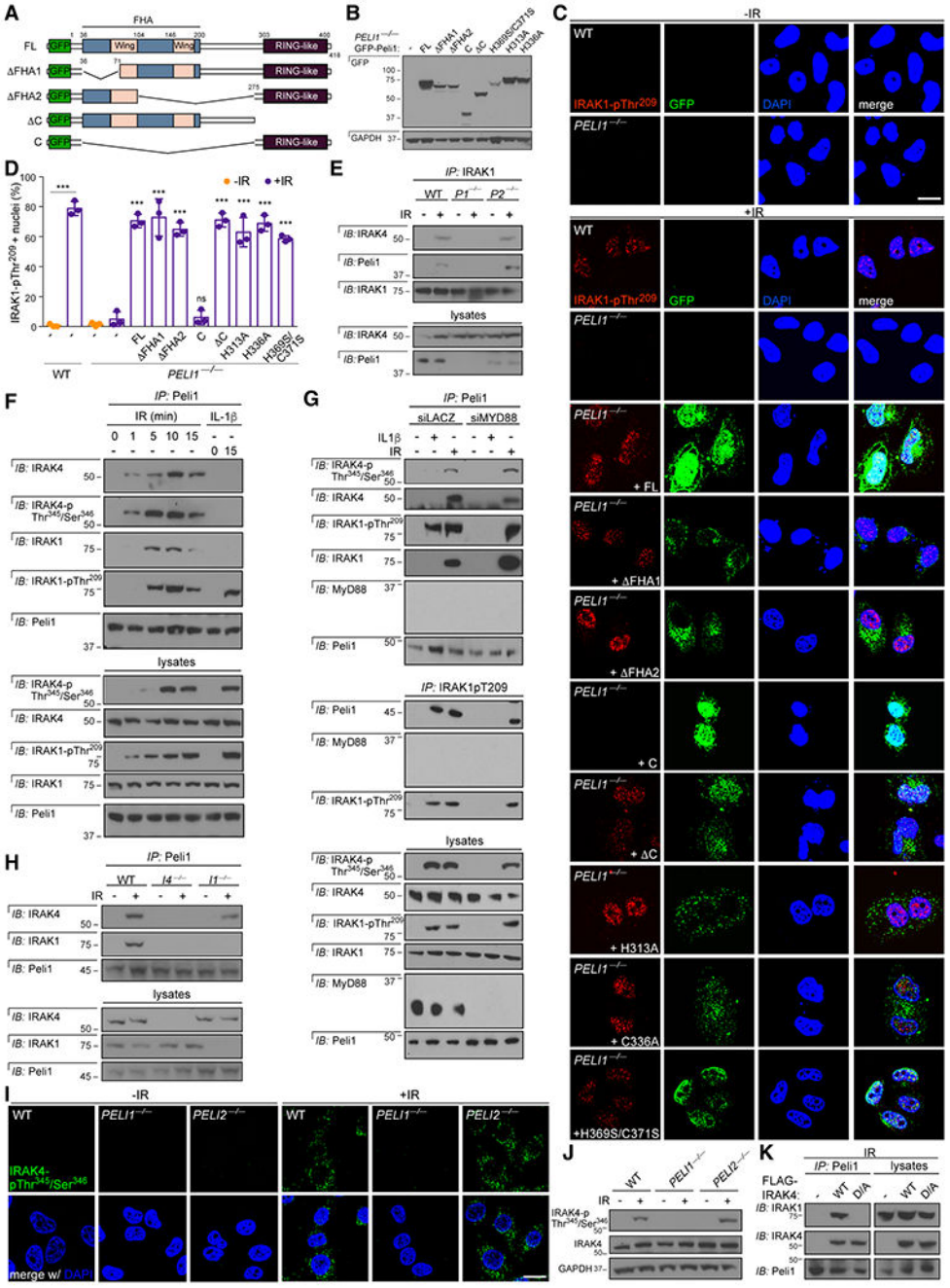

Fig. 7. Peli1 functionally substitutes for MyD88 in non-canonical IRAK1 signaling.

(**A**) Diagrams of full-length (FL) GFP-Peli1 and deletion constructs (54). FHA, forkhead-associated; RING-like, really interesting new gene-like (catalytic domain). See also fig. S7D. (**B**) Expression levels of GFP-Peli1 constructs depicted in (A) in reconstituted *PELI1*$^{-/-}$ cells as analyzed in (C-D). (**C and D**) Parent (WT) and *PELI1*$^{-/-}$ cells transfected with or without GFP-Peli1 constructs (see (A)) were treated with or without IR (7.5 Gy), fixed at 15 min and imaged by confocal microscopy (C), from which the percentage of cells with IRAK1-pThr^{209} signal-positive nuclei were quantified (D). Images are representative, and

data are means ± SD of $n = 3$ independent experiments, with at least 80 cells analyzed per condition. Statistical significance vs. bar 4: ***$p < 0.001$; ns, non-significant; two-tailed Student's t-test. (**E**) Parent, *PELI1*$^{-/-}$ and *PELI2*$^{-/-}$ cells were treated with or without IR (7.5 Gy), harvested at 15 min, immunoprecipitated with IRAK1 antibody and analyzed by western blot. (**F**) Hela cells were treated with or without IR (7.5 Gy) or IL-1β(0.1 μg/mL), harvested at indicated time points, immunoprecipitated with Peli1 antibody and analyzed by western blot. (**G**) Hela cells transfected with indicated siRNA were treated with or without IR (7.5 Gy) or IL-1β(0.1 μg/mL), harvested at 15 min, and Peli1 immunoprecipitates (top) and IRAK1-pThr^{209} immunoprecipitates (middle) were analyzed by western blot. (**H**) Parent, *IRAK4*$^{-/-}$ (*I4*$^{-/-}$) and *IRAK1*$^{-/-}$ (*I1*$^{-/-}$) cells were treated with or without IR (7.5 Gy), harvested at 15 min, and Peli1 immunoprecipitates were analyzed by western blot. (**I**) Cells of indicated genotypes were treated with or without IR (7.5 Gy), fixed at 15 min and stained with IRAK4-pThr^{345}/Ser^{346} antibody and DAPI. Images are representative of at least 50 cells per condition over $n = 2$ independent experiments. (**J**) Cells as described in (I) were harvested at 15 min after IR and analyzed by western blot. (**K**) *IRAK4*$^{-/-}$ HeLa cells transfected with indicated FLAG-IRAK4 constructs were irradiated (7.5 Gy) and harvested at 10 min. Peli1 immunoprecipitates were analyzed by western blot. Blots in (B, E, F-H, J and K) are representative of at least $n = 2$ independent experiments. Scale bars in (C and I), 5 μm.

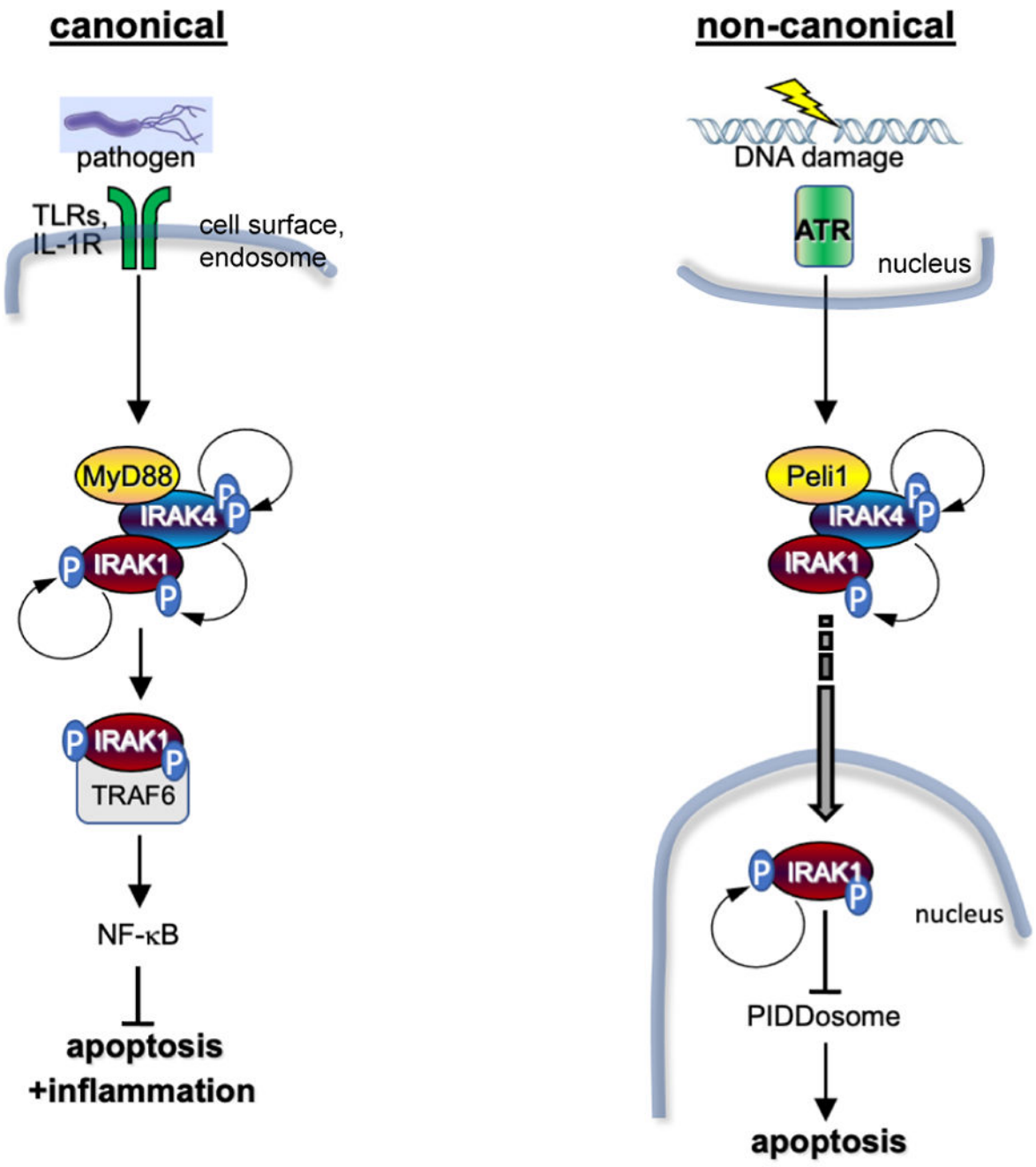

Fig. 8. Two vertebrate IRAK signaling pathways.

Diagrams of the TLR/IL-1R innate immune pathway (canonical, left) and DSB-induced anti-apoptotic pathway (non-canonical, right) highlighting distinct transduction mechanisms and cellular dynamics upstream and downstream of the IRAK/IRAK1 core module. See text for details.